SUPPORTING INFORMATION

Cadmium and silver complexes of a pyridine containing ligand: syntheses, structural studies, biological activity and docking studies

Azza A. Hassoon[a*], Stacey J. Smith[b], Roger G. Harrison[b]

[a]*Chemistry Department, Faculty of Science, Mansoura University, Egypt*
[b]*Department of Chemistry & Biochemistry, Brigham Young University, USA*

Corresponding authors: azza_ahmed@hotmail.com, azza_ahmed@mans.edu.eg

1. Experimental section

1.1. Materials and Methods

All chemicals and solvents utilized in the study were of the highest purity (BDH and/or AR quality) and were used as received without further purification. The substances included ***TPT*** (2,4,6-tri-(2-pyridyl)-1,3,5-triazine), $AgClO_4$, $CdCl_2$, dimethylsulphoxide (DMSO), diethyl ether (BDH or Merck), EtOH, nitric acid (Aldrich), silver nitrate of analytical grade, and tetrabutylammonium perchlorate (TBAP) as the supporting electrolyte. All glassware is immersed in a chromic solution, washed with distilled water, and then dried in an oven at 120 ºC.

1.2. Instruments

IR spectra were recorded utilizing KBr discs in the 4000–400 cm^{-1} range on Bruker IFS-66 FTIR Spectrometer. Cadmium content was determined by PerkinElmer, Optima 2000 ICP-OES spectrometer. Chloride ions were determined gravimetrically using the AgCl precipitate by using $AgNO_3$ as precipitating agent. One-dimensional (^1H, ^{13}C and ^{31}P) and two-dimensional (^1H–^1H COSY (COrrelated SpectroscopY) and ^1H–^{13}C HSQCAD (Heteronuclear Single Quantum Coherence)) NMR spectra were recorded in DMSO-d_6 on a Bruker Bio Spin AG spectrometer at 500 MHz. The chemical shifts are reported relative to TMS using the solvent signal (δ ^1H = 2.50 ppm; δ ^{13}C = 39.50 ppm) as reference. NMR data were obtained from freshly prepared concentrated solutions. The UV–vis Shimadzu spectrophotometer (UV-2600) was utilized to obtain the electronic spectra of the complexes dissolved in DMSO at ambient temperature in the 200–700 nm range. Fluorescence emission spectra for solutions of ***TPT*** and complexes in DMSO were recorded with excitation wavelength of 200 nm at room temperature on Photon Technology Inc. Fluorimeter equipped with quartz cuvettes of 1 cm path length. Melting points were determined using a Stuart Scientific SMP30 instrument. The electronic conductance was measured using 1 mM solution in DMSO with Jenway 4010 conductivity meter at room temperature. The electrochemical cell used as conventional three electrode type saturated calomel electrode (SCE) as a reference electrode and Pt wire and glass carbon as auxiliary and working electrode and 0.1 M tetrabutylammonium perchlorate (TBAP) as electrolyte. A scan rate of 50 mV s^{-1} was employed by using BAC Epsilon Electrochemical Instrument. CHN were

carried out by Microanalytical Services. Thermo gravimetric analysis (TGA) was carried out in the range 20–700°C with a Shimadzu TGA-50 analyser at a heating rate of 10°C min^{-1} and nitrogen flow rate of 1 min^{-1}.

1.3. Powder X-ray diffraction

Powder X-ray diffraction data were acquired by Pan Analytical X'Pert Pro Powder X-Ray Diffraction Instrument. The interplanar spacing (d) has been determined by measuring the positions of intense peaks using Bragg's equation $n\lambda = 2d\ Sin\Theta$ (where λ = 1.5405980 ˚A). The size of the crystallites can be determined by analyzing the XRD patterns and calculating the Full Width at Half Maximum (FWHM) of the characteristic peaks using the Deby-Scherrer Equation. The equation is $D = K.\lambda / \beta.\cos\theta$. The particle size of the crystal gain is represented by D, the constant for Cu grid is denoted as K (with a value of 0.94), the X-ray wavelength is represented by λ (with a value of 0.1541 nm), the Bragg diffraction angle is denoted as θ, and the integral peak width is represented by ß. The particle size was determined based on the peak with the highest intensity in comparison to the other peaks.

1.4. X-ray studies

1.4.1. Refinement

A pale yellow crystal was collected in oil at room temperature and positioned at the end of a polyimide loop. The crystal was positioned in a flow of chilled nitrogen and aligned in the X-ray beam with the help of a video camera. X-ray diffraction data at 100 K were acquired using a MACH3 four-circle goniometer connected to a Bruker Apex II CCD detector with a Bruker-Nonius FR591 rotating anode X-ray source emitting Cu K_α radiation (λ = 1.54178 Å), including φ- and ω- scans. The Bruker APEX3 suite processed the data, reflection intensities were combined using the program SAINT, and absorption adjustments were made to the intensities through a multi-scan technique using the program SADABS. The structure was determined using dual-space approaches in SHELXT [1] and refined against F2 on all data through full-matrix least squares with SHELXL-2014 [2], employing proven refinement techniques. [3]

Anisotropic refinement was performed on all atoms except hydrogen. Hydrogen atom locations, except those on the ethanol alcohol groups, were geometrically computed and refined using a riding model. The locations of the remaining hydrogen atoms were determined using the difference Fourier synthesis and then revised semi-freely with the use of suitable distance constraints. The isotropic displacement parameters for all hydrogen atoms were restricted to 1.2

times the Ueq value of the atom they are connected to, except for methyl hydrogens which were set at 1.5 times the U_{eq} value.

The details of the crystal of compound **Q6** in Cambridge database is as follows:

Data Citation: Azza A. Hassoon, Stacey Smith, Roger Harrison, CCDC 1509097: Experimental Crystal Structure Determination, DOI: 10.5517/ccdc.csd.cc1mnbk5. Refcode: EFUKEZ

1.5. Biological studies

1.5.1. Determination of cytotoxic and antimicrobial activities

MCF-7 cell line, derived from the mammary gland, and MCF-10A Cell line (normal cell line) were acquired from ATCC through VACSERA, a biological products and vaccines holding company based in Cairo, Egypt. The cell lines were utilized to assess the inhibitory impact of substances on cell proliferation by the MTT test. This colorimetric assay relies on the transformation of the yellow tetrazolium bromide (MTT) into a purple formazan derivative by mitochondrial succinate dehydrogenase in living cells. The cell line was grown in RPMI-1640 media supplemented with 10% fetal bovine serum. The antibiotics used were 100 units/ml of penicillin and 100 µg/ml of streptomycin, incubated at 37°C in a 5% CO_2 environment. The cell line was cultured in a 96-well plate with a density of 1.0 x 10^4 cells/well at 37°C for 48 hours in a 5% CO_2 environment. Following incubation, the cells were exposed to varying concentrations of complexes and incubated for 24 hours. After 24 hours of drug treatment, 20 microliters of MTT solution at a concentration of 5 milligrams per milliliter was added and incubated for 4 hours. 100 µl of Dimethyl sulfoxide (DMSO) is added to each well to dissolve the purple formazan. The colorimetric assay is quantified at an absorbance of 570 nm using a plate reader (EXL 800, USA). The percentage of relative cell viability was determined using the formula: (A570 of treated samples/A570 of untreated sample) X 100.

The synthesized compounds were evaluated for their antimicrobial activity against Staphylococcus aureus (gram-positive bacteria) and Escherichia coli (gram-negative bacteria). Furthermore, the compounds were investigated for their antifungal properties against Candida albicans. Each compound was dissolved in DMSO to generate separate solutions with a concentration of 1 mg/ml. Paper discs made of Whatman filter paper were cut to a standard size of 5 cm and sterilized in an autoclave. The paper discs, saturated with the specified concentration

of the complex solution, were aseptically positioned on petri dishes filled with nutrient agar media (consisting of agar 20 g, beef extract 3 g, and peptone 5 g) inoculated with Staphylococcus aureus, E. coli, and Candida albicans. The petri plates were placed in an incubator set at 36 degrees Celsius, and the inhibition zones were measured 24 hours later. Each treatment was duplicated thrice. The antibacterial properties of the conventional antibiotic Ciprofloxacin and antifungal Colitrimazole were tested using the same method, concentration, and solvents as previously described. The activity index for the complex was determined using the following formula:

$$\%\ Activity\ Index = \frac{Zone\ of\ inhibition\ by\ test\ compound\ (diametre)}{Zone\ of\ inhibition\ by\ standard\ (diametre)} \text{x}100$$

1.6. Molecular docking simulation

1.6.1. Protein Structure Preparation

The 3D structures of the target proteins cyclin-dependent kinase 2 (CDK2, UniProt: Q63699), cyclin-dependent kinase 6 (CDK6, UniProt: F1MA87), signal transducer and activator of transcription 3 (STAT3, UniProt: P52631), and beta-lactamases from Escherichia coli (PDB: 4OQG) and Staphylococcus aureus (UniProt: Q7BWD2) were retrieved as Protein Data Bank (PDB) file format, then Potential binding sites on each protein were predicted using the DeepSite algorithm.[4]

1.6.2. Ligand Preparation

The 3D structures of ligand compounds were built and pre-optimized using Avogadro 1.2.0 [5] with the Universal Force Field and Merck Molecular Force Field (MMFF94) methods, assigning Gasteiger-Marsili charges.

1.6.3. Molecular Docking

Molecular docking of the ligands into the predicted binding sites of each target protein was performed using the HDock rigid protein-ligand docking algorithm.[6] HDock employs a hybrid scoring function combining desolvation, van der Waals, and electrostatic energies. The top-scoring docking poses were further evaluated for binding free energy calculations using the PRODIGY web server. [7,8]

1.6.4. Visualization and Analysis

The top-scoring docked ligand-protein complexes were visualized and analyzed using BIOVIA Discovery Studio Visualizer 2020. [9]

1.6.5. Solution stability

A stock solution of 5 mM of each complex was prepared in DMSO-d_6 (to improve solubility) followed by appropriate dilutions with phosphate-buffered saline (PBS): pH 7.4, 137 mM NaCl, 2.7 mM KCl, 10 mM Na_2HPO_4 and 1.8 mM K_2HPO_4) to obtain the desired complex concentration in the final volume of samples. The ^{1}H-NMR spectra of the complexes were measured with increasing time (over 24 h) at room temperature.

1.7. Synthesis of metal complexes:

1.7.1. Cadmium compound (Q1): ***TPT*** ligand (1 mmol, 0.31 g) was dissolved in 20 ml ethanol to which on 20 ml alcoholic solution of anhydrous $CdCl_2$ (3 mmol, 0.55 g) was added. The mixture was allowed to stir under reflux for 24 h at 80 ^{o}C till dissolving all amount of $CdCl_2$. The pH of the solution was found equal to 6. White complex with chemical formula $[Cd_3(\boldsymbol{TPT})Cl_6]$.EtOH complex (**Q1**) was obtained.

$[Cd_3(\boldsymbol{TPT})Cl_6]$.EtOH (Q1): yield 65 %; color white powder; m.p. >400 ^{o}C. Anal.Calcd for $C_{20}H_{18}Cl_6Cd_3N_6O$ (908.34): C: 26.4; H: 1.99; N: 9.25; Cl: 23.4; Cd: 41.7 %. Found: C: 27.1; H: 2.2; N: 10.7; Cl: 22.7; Cd: 41.5 %, μ_{eff} (dia.) and conductivity: 23.8 Ω^{-1} cm^2 mol^{-1}. IR (KBr, cm^{-1}): 3344-3464 υ(OH), 1605 δ(OH), 3074 υ(CH) aromatic, 1452, 1545, 1574 υ(C=C, C=N), 638 δ(C=N), 417 (Cd-N)pyr, 424 (Cd-N)triaz. ^{1}H NMR for ***TPT*** (500 MHz, DMSO-d_6) (ppm): 9.01 (d, 1H), 8.91 (d, 1H), 8.34 (t, 1H), 7.97 (t, 1H). ^{13}C NMR (125 MHz, DMSO-d_6) (ppm): 152.86 (C2), 126.09 (C6).

1.7.2. Silver compounds (Q2-Q7): The reaction of ***TPT*** with $AgClO_4$ in a different (Ag:L) molar ratio in absolute ethanol afforded four complexes (**Q2–Q5**).

$[Ag(\boldsymbol{TPT})(H_2O)](ClO_4)$ (Q2): ***TPT*** (0.16 g, 0.5 mmol) in EtOH (15 ml) was added to silver perchlorate (0.11 g, 0.5 mmol) in EtOH (10 ml). The reaction mixture was stirred at 80 ^{o}C in the dark for 2 h and yellowish-orange solid is obtained.

Yield 95 %; color yellowish-orange powder; m.p. >400 °C. Anal.Calcd for $C_{18}H_{14}N_6ClO_5Ag$ (537.67): C: 40.2; H: 2.6; N: 15.6 %. Found: C: 40.3; H: 2.5; N: 15.9 %, μ_{eff} (dia.) and conductivity: 36 Ω^{-1} cm^2 mol^{-1}. IR (KBr, cm^{-1}): 3344-3464 υ(OH), 1578 δ(OH), 3081 υ(CH) aromatic, 1470, 1535, 1540 υ(C=C, C=N), 673 δ(C=N), 412 (Ag-N)pyr, 490 (Ag-N)triaz, 516 (Ag-O), 1093, 623 ν(ClO_4). ^{1}H NMR for ***TPT*** (500 MHz, DMSO-d_6) (ppm): 8.95 (d, 1H), 8.71 (d, 1H), 8.18 (t, 1H), 7.77 (t, 1H). ^{13}C NMR (125 MHz, DMSO-d_6) (ppm): 169.14 (C1), 150.82 (C2), 149.60 (C3), 138.88 (C4), 128.57 (C5), 125.34 (C6).

$[Ag_3(TPT)_2(ClO_4)(H_2O)](H_2O)_2(ClO_4)_2$ (Q3): ***TPT*** (0.16 g, 0.5 mmol) in EtOH (15 ml) was added to silver perchlorate (0.22 g, 1 mmol) in EtOH (10 ml). The reaction mixture was stirred at 80 °C in the dark for 2 h and pale yellow solid is obtained.

Yield 92 %; color pale yellow powder; m.p. 320 °C. Anal.Calcd for $C_{36}H_{30}N_{12}Ag_3O_{15}Cl_3$ (1300.68): C: 33.2; H: 2.3; N: 12.9 %. Found: C: 32.7; H: 1.96; N: 12.9 %, μ_{eff} (dia.) and conductivity: 64 Ω^{-1} cm^2 mol^{-1}. IR (KBr, cm^{-1}): 3344-3464 υ(OH), 1571 δ(OH), 3082 υ(CH) aromatic, 1477, 1535 υ(C=C, C=N), 669 δ(C=N), 410 (Ag-N)pyr, 459 (Ag-N)triaz, 570 (Ag-O), 1018, 1052, 1097, 625, 669, 746 ν(ClO_4). ^{1}H NMR for ***TPT*** (500 MHz, DMSO-d_6) (ppm): 8.96 (d, 1H), 8.77 (d, 1H), 8.19 (t, 1H), 7.81 (t, 1H). ^{13}C NMR (125 MHz, DMSO-d_6) (ppm): 169.02 (C1), 150.99 (C2), 149.39 (C3), 139.04 (C4), 128.74 (C5), 125.46 (C6).

$[Ag_2(TPT)_3(ClO_4)](H_2O)_3(ClO_4)$ (Q4): silver perchlorate (0.05 g, 0.25 mmol) in EtOH (5 ml) was added to ***TPT*** (0.16 g, 0.5 mmol) in EtOH (10 ml). The reaction mixture was stirred at 80 °C in the dark for 2 h and deep yellow solid is obtained.

Yield 89 %; color deep yellow powder; m.p. 380 °C. Anal.Calcd for $C_{54}H_{42}N_{18}Ag_2O_{11}Cl_2$ (1405.70): C: 46.1; H: 3.0; N: 17.9 %. Found: C: 45.9; H: 2.3; N: 18.2 %, μ_{eff} (dia.) and conductivity: 44 Ω^{-1} cm^2 mol^{-1}. IR (KBr, cm^{-1}): 3344-3464 υ(OH), 1571 δ(OH), 3068 υ(CH) aromatic, 1440, 1468, 1537 υ(C=C, C=N), 665 δ(C=N), 407 (Ag-N)pyr, 495 (Ag-N)triaz, 561 (Ag-O), 1000, 1049, 10933, 623, 669, 739 ν(ClO_4). ^{1}H NMR for ***TPT*** (500 MHz, DMSO-d_6) (ppm): 8.98 (d, 1H), 8.64 (d, 1H), 8.19 (t, 1H), 7.72 (t, 1H). ^{13}C NMR (125 MHz, DMSO-d_6) (ppm): 169.34 (C1), 150.59 (C2), 149.98 (C3), 138.67 (C4), 128.34 (C5), 125.20 (C6).

$[Ag_2(TPT)_2(ClO_4)](H_2O)(ClO_4)$ (Q5): Silver perchlorate (0.11 g, 0.5 mmol) in EtOH (5 ml) was added to alcoholic solution of 2,2'-bipyridine (0.08 g , 0.5 mmol; 5 ml). To the formed pale

yellow solid complex, ***TPT*** (0.16 g, 0.5 mmol) in EtOH (10 ml) was added. The reaction mixture was stirred in the dark for 3 h and the deep yellow solid produced.

Yield 90 %; color yellowish-orange powder; m.p. 400 ^{o}C. Anal.Calcd for $C_{36}H_{26}N_{12}O_9Ag_2Cl_2$ (1057.33): C: 40.9; H: 2.5; N: 15.9 %. Found: C: 40.7; H: 2.0; N: 16.0 %, μ_{eff} (dia.) and conductivity: 36 Ω^{-1} cm^2 mol^{-1}. IR (KBr, cm^{-1}): 3344-3464 υ(OH), 1576 δ(OH), 3086 υ(CH) aromatic, 1440, 1470, 1541 υ(C=C, C=N), 678 δ(C=N), 413 (Ag-N)pyr, 494 (Ag-N)triaz, 559 (Ag-O), 1001, 1053, 1093, 625, 673, 744 ν(ClO_4). ^{1}H NMR for ***TPT*** (500 MHz, DMSO-d_6) (ppm): 8.98 (d, 1H), 8.75 (d, 1H), 8.22 (t, 1H), 7.79 (t, 1H). ^{13}C NMR (125 MHz, DMSO-d_6) (ppm): 169.22 (C1), 150.76 (C2), 149.83 (C3), 138.82 (C4), 128.50 (C5), 125.28 (C6). 2,2'-bipyridine did not participate in coordination.

[Ag(*TPT*)(PPh_3)$_2$](ClO_4).EtOH (Q6): Silver perchlorate (0.11 g, 0.5 mmol) in EtOH (5 ml) was added to alcoholic solution of triphenylphosphine (PPh_3) (0.13, 0.5 mmol; 10 ml). To the colorless solution obtained, ***TPT*** (0.16 g, 0.5 mmol) in EtOH (10 ml) was added. The reaction mixture was stirred in the dark for 2 h and the yellow solid produced was filtered off, washed with EtOH, Et_2O and dried in a vacuum desiccator over anhydrous P_4O_{10}. The yellow solution was allowed to evaporate slowly in air. Near the dryness of the solution, Pale yellow crystals, suitable for X-ray analysis, separated out. Yield 90 %; color yellow powder; m.p. >400 ^{o}C for $C_{56}H_{48}N_6P_2O_5AgCl$ (1090.91): μ_{eff} (dia.) and conductivity: 57.3 Ω^{-1} cm^2 mol^{-1}. IR (KBr, cm^{-1}): 3344-3464 υ(OH), 1576 δ(OH), 3082 υ(CH) aromatic, 1443, 1470, 1539 υ(C=C, C=N), 669 δ(C=N), 407 (Ag-N)pyr, 492 (Ag-N)triaz, 1093, 623 ν(ClO_4). ^{1}H NMR for ***TPT*** (500 MHz, DMSO-d_6) (ppm): 8.91 (d, 1H), 8.68 (d, 1H), 8.15 (t, 1H), 7.73 (t, 1H), 7.33–7.59 (m, 18H, H(PPh_3). ^{13}C NMR (125 MHz, DMSO-d_6) (ppm): 169.16 (C1), 150.78 (C2), 149.66 (C3), 138.86 (C4), 128.55 (C5), 125.31 (C6), 128.73–133.46 (s, 18C, C(PPh3). ^{31}P {^{1}H} (202.5 MHz, DMSO-d_6) (ppm): δ 25.56 (s).

[Ag$_2$(*TPT*)(phen)$_2$(ClO_4)](H_2O)$_2$(ClO_4) (Q7): Silver perchlorate (0.11 g, 0.5 mmol) in EtOH (5 ml) was added to alcoholic solution of 1,10-phenanthroline (phen) (0.09 g , 0.5 mmol; 5 ml). To the formed yellow solid complex, ***TPT*** (0.16 g, 0.5 mmol) in EtOH (10 ml) was added. The reaction mixture was stirred in the dark for 2 h and the yellowish-orange solid produced.

Yield 90 %; color yellowish-orange powder; m.p. 400 ^{o}C. Anal.Calcd for $C_{42}H_{32}N_{10}O_{10}Ag_2Cl_2$ (1123.43): C: 44.9; H: 2.9; N: 12.5 %. Found: C: 44.7; H: 2.2; N: 13.1 %, μ_{eff} (dia.) and conductivity: 45 Ω^{-1} cm^2 mol^{-1}. IR (KBr, cm^{-1}): 3344-3464 υ(OH), 1571 δ(OH), 3076 υ(CH)

aromatic, 1473, 1514, 1540 υ(C=C, C=N), 671 δ(C=N), 417 (Ag-N)pyr, 491 (Ag-N)triaz, 573 (Ag-O), 1052, 1091, 1142, 623, 675, 725 ν(ClO_4). ^{1}H NMR for ***TPT*** (500 MHz, DMSO-d_6) (ppm): 8.99 (d, 1H), 8.65 (d, 1H), 8.19 (t, 1H), 7.75 (t, 1H), for phenanthroline: 9.12 (d, 1H, J_{HA} = 6.5 Hz), 8.79 (d, 1H, J_{HB} = 9.5 Hz), 8.23 (s, 1H), 8.01 (dd, 1H). ^{13}C NMR (125 MHz, DMSO-d_6) (ppm): 169.23 (C1), 150.65 (C2), 149.86 (C3), 138.51 (C4), 128.49 (C5), 125.00 (C6), for phenanthroline: 151.30 (C1), 141.94 (C2), 138.78 (C3), 128.01 (C4), 127.25 (C5), 125.31 (C6).

All produced complexes were filtered off, washed with EtOH, Et_2O and dried in a vacuum desiccator over anhydrous P_4O_{10}.

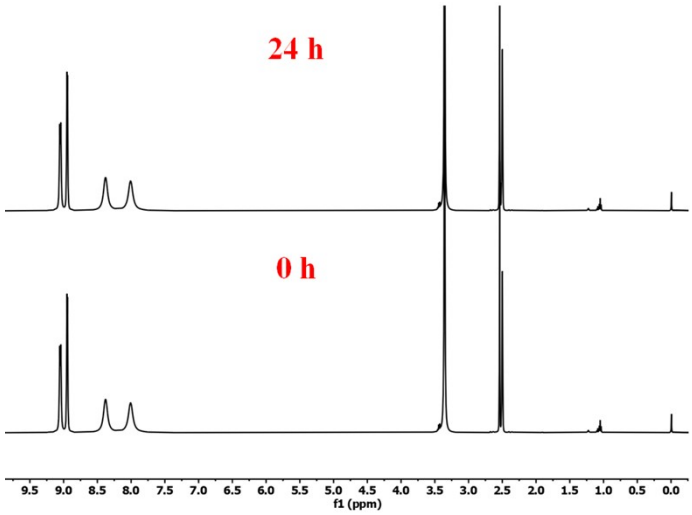

Figure S1. Time dependence of ^{1}H-NMR spectra of **Q1**

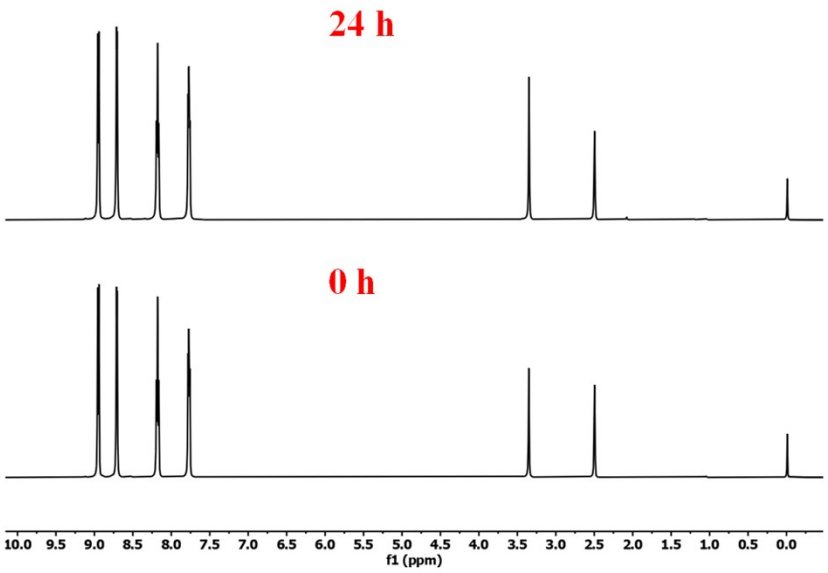

Figure S2. Time dependence of ^{1}H-NMR spectra of **Q2** (500 MHz, DMSO)

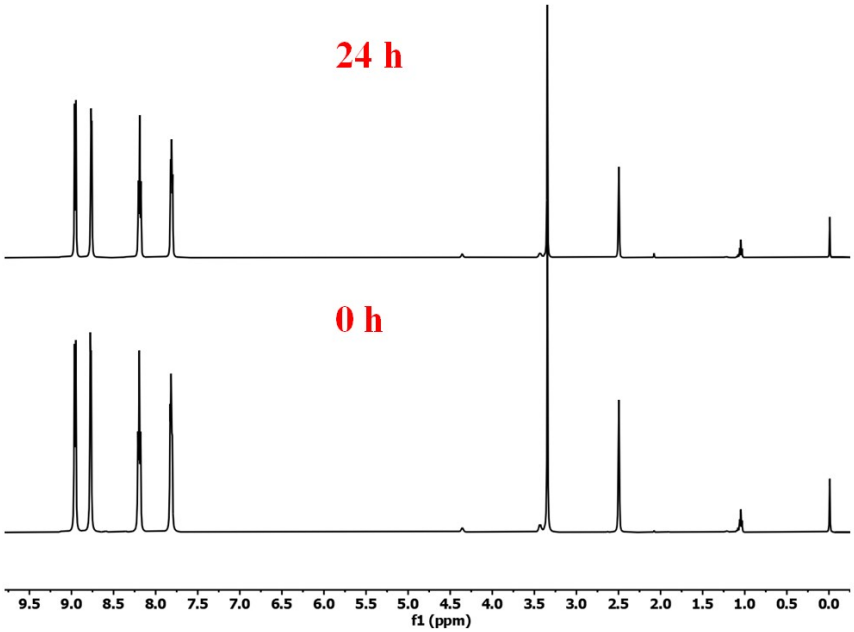

Figure S3. Time dependence of ^{1}H-NMR spectra of **Q3** (500 MHz, DMSO)

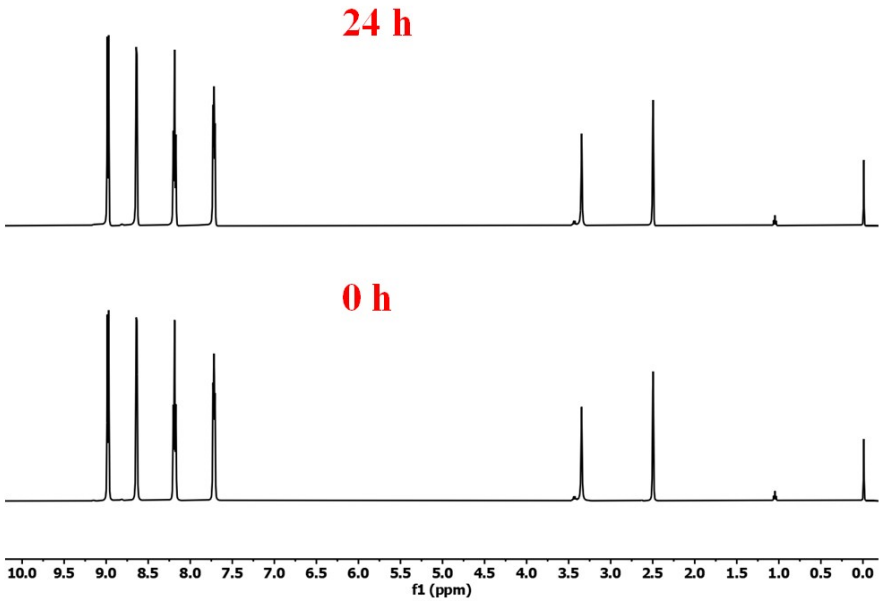

Figure S4. Time dependence of ^{1}H-NMR spectra of **Q4** (500 MHz, DMSO)

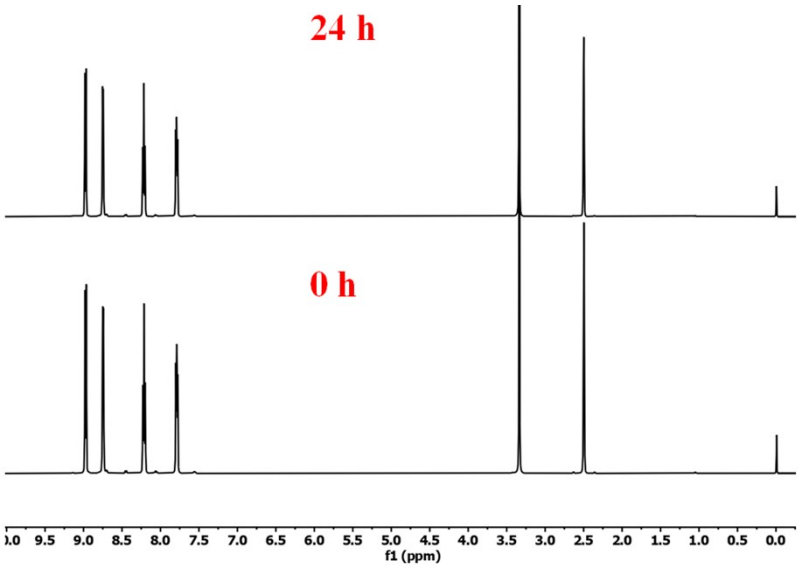

Figure S5. Time dependence of ^{1}H-NMR spectra of **Q5** (500 MHz, DMSO)

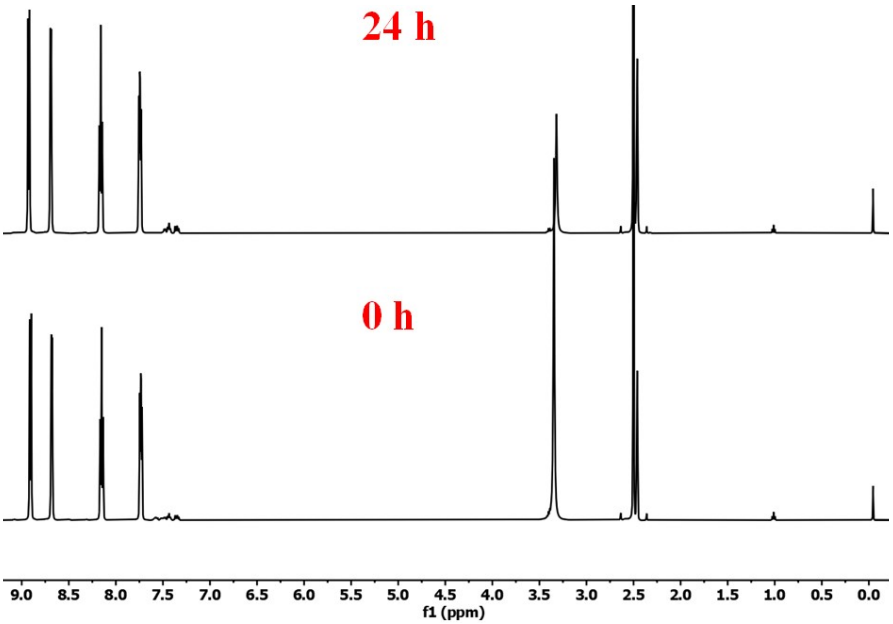

Figure S6. Time dependence of ^{1}H-NMR spectra of **Q6** (500 MHz, DMSO)

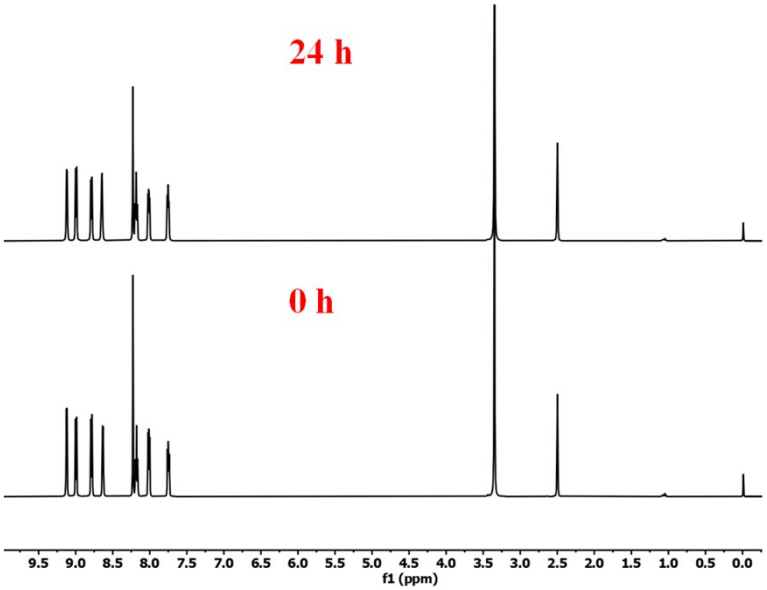

Figure S7. Time dependence of ^{1}H-NMR spectra of **Q7** (500 MHz, DMSO)

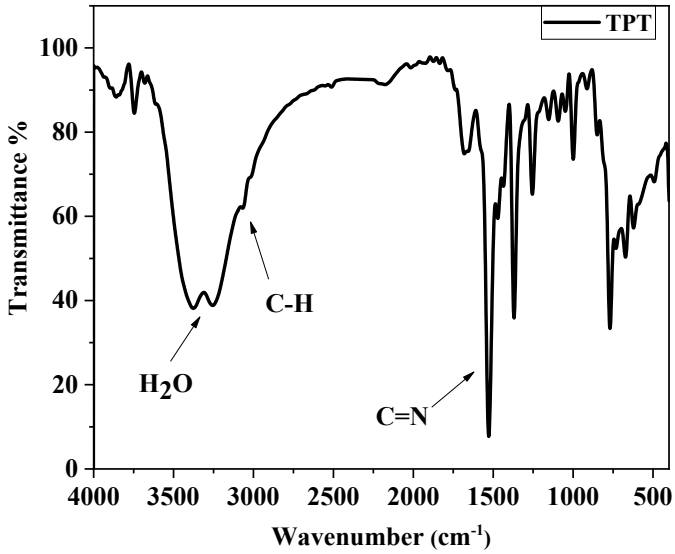

Figure S8. IR spectrum of ***TPT.*** [10]

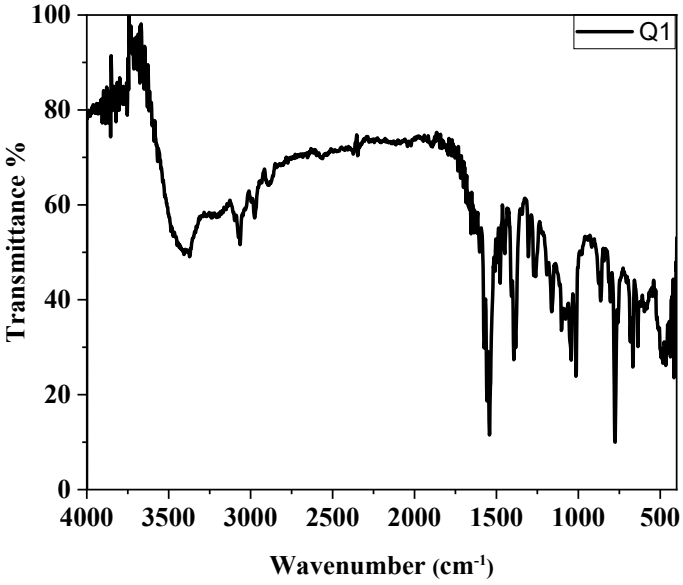

Figure S9. IR spectrum of complex **Q1**

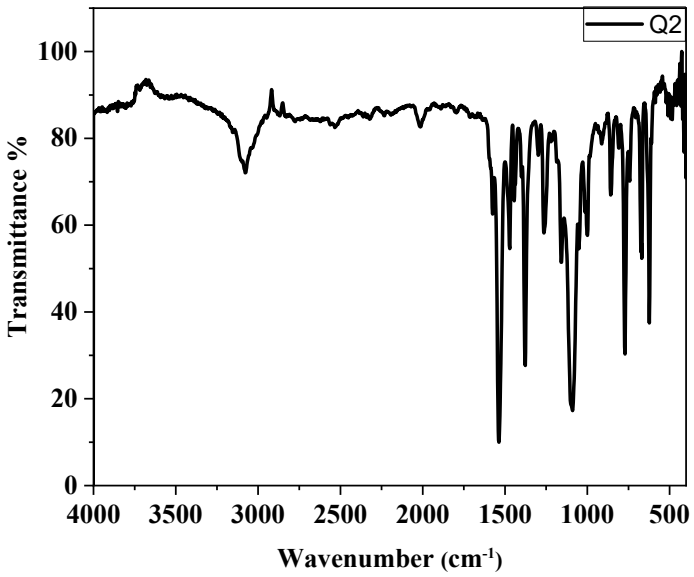

Figure S10. IR spectrum of complex **Q2**

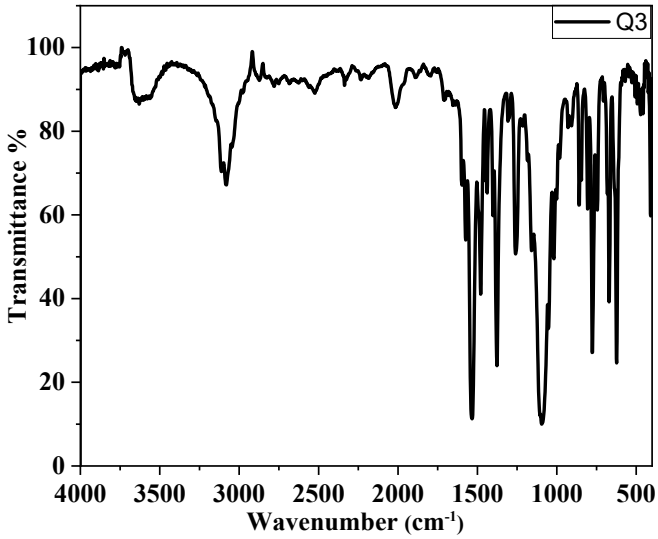

Figure S11. IR spectrum of complex **Q3**

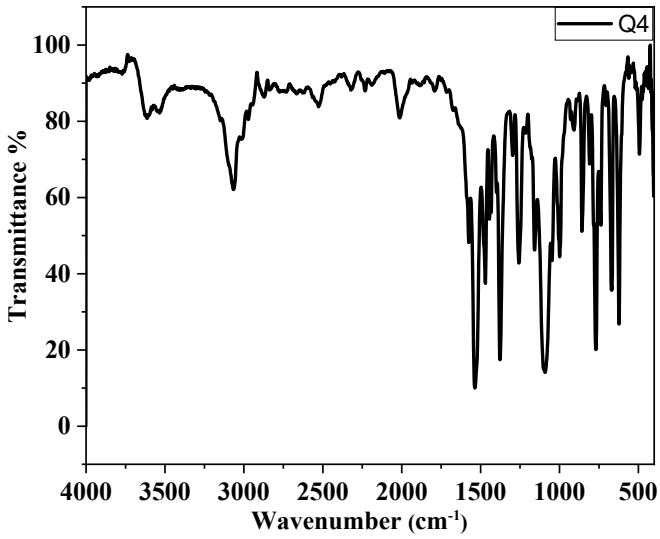

Figure S12. IR spectrum of complex **Q4**

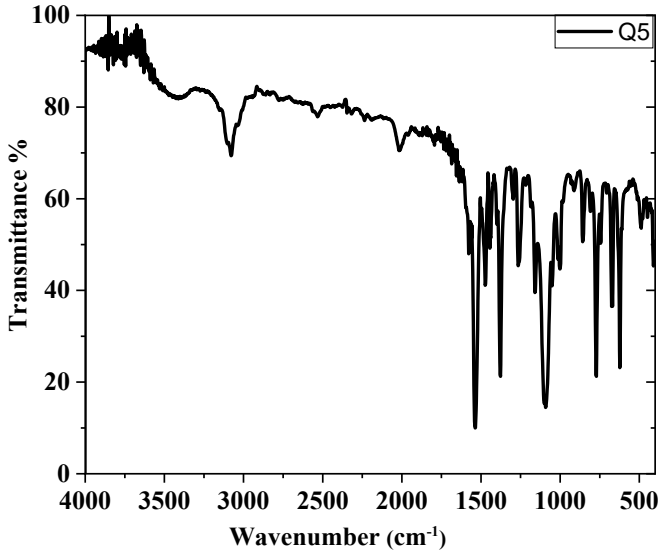

Figure S13. IR spectrum of complex **Q5**

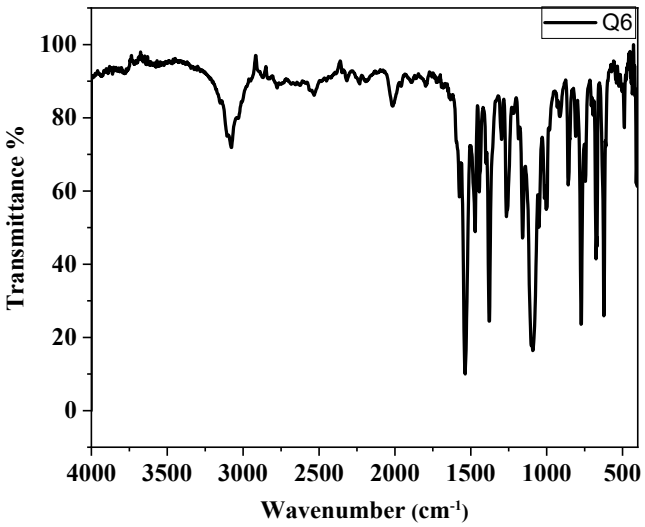

Figure S14. IR spectrum of complex **Q6**

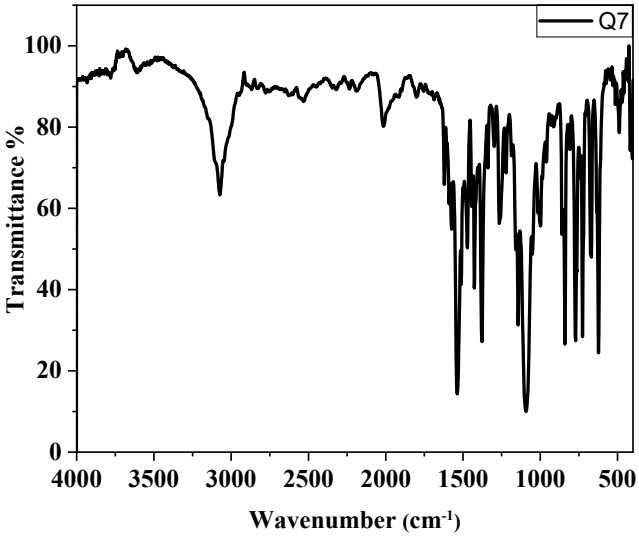

Figure S15. IR spectrum of complex **Q7**

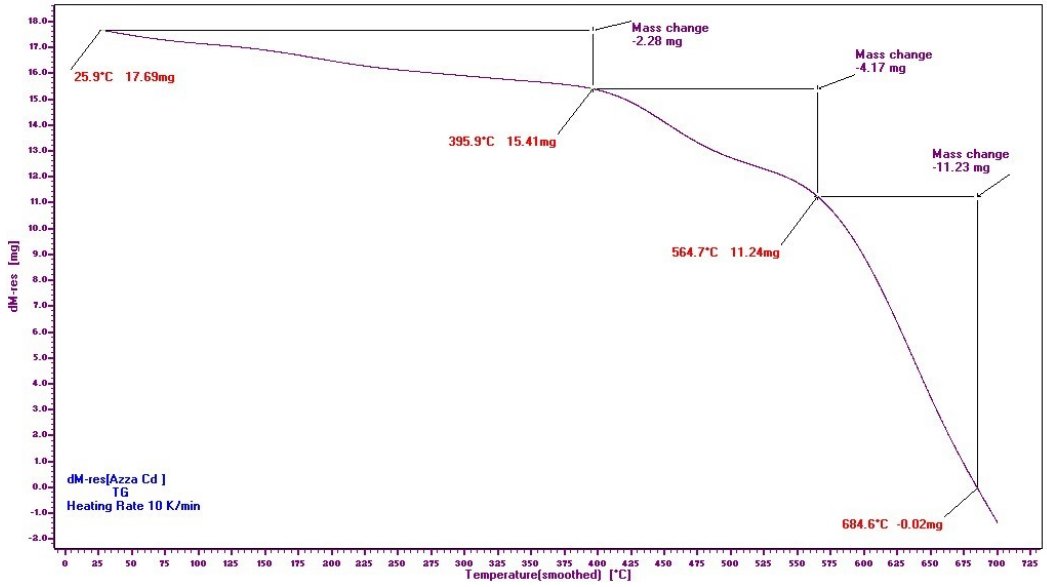

Figure S16. The TGA curve of the cadmium complex **Q1**

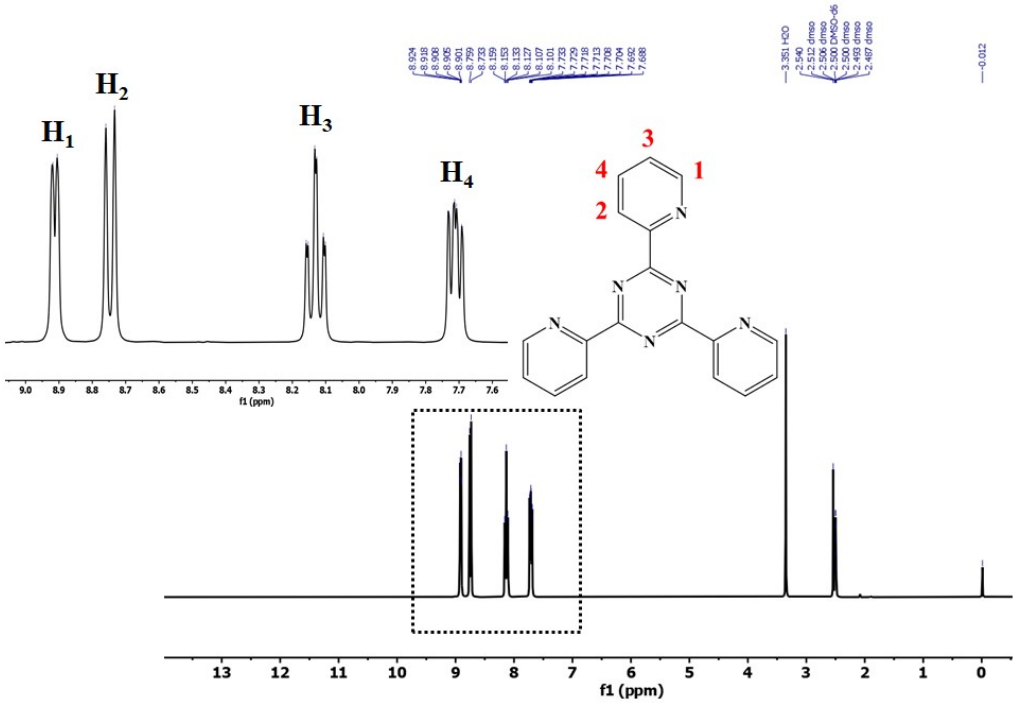

Figure S17. ^{1}H-NMR spectra of ***TPT*** ligand (500 MHz, DMSO-d_6).

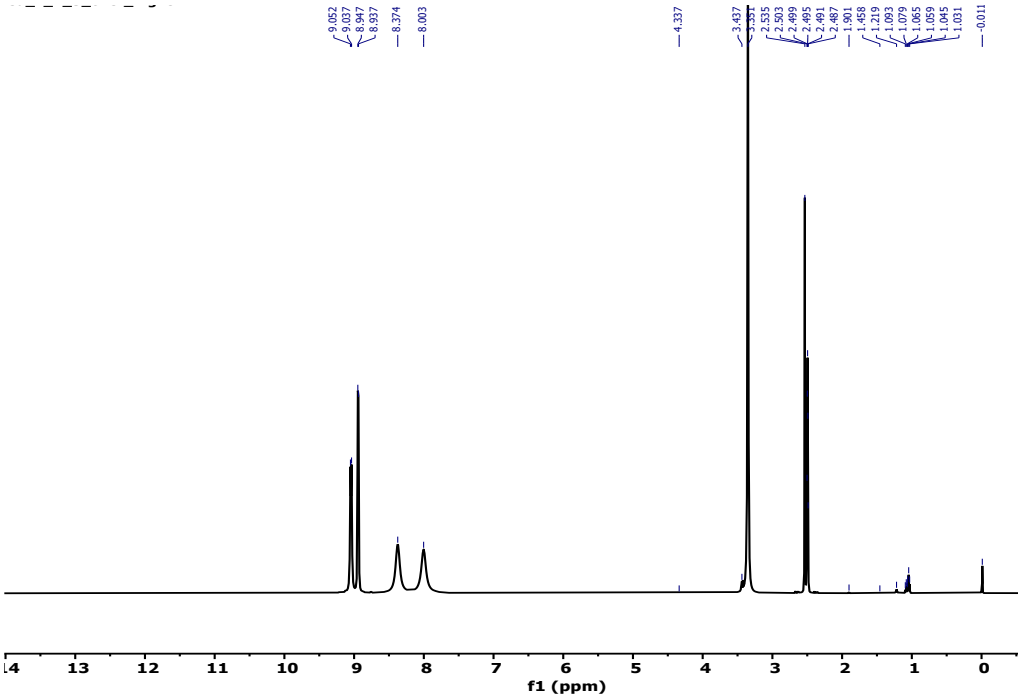

Figure S18. ^{1}H-NMR spectra of complex **Q1** (500 MHz, DMSO-d_6).

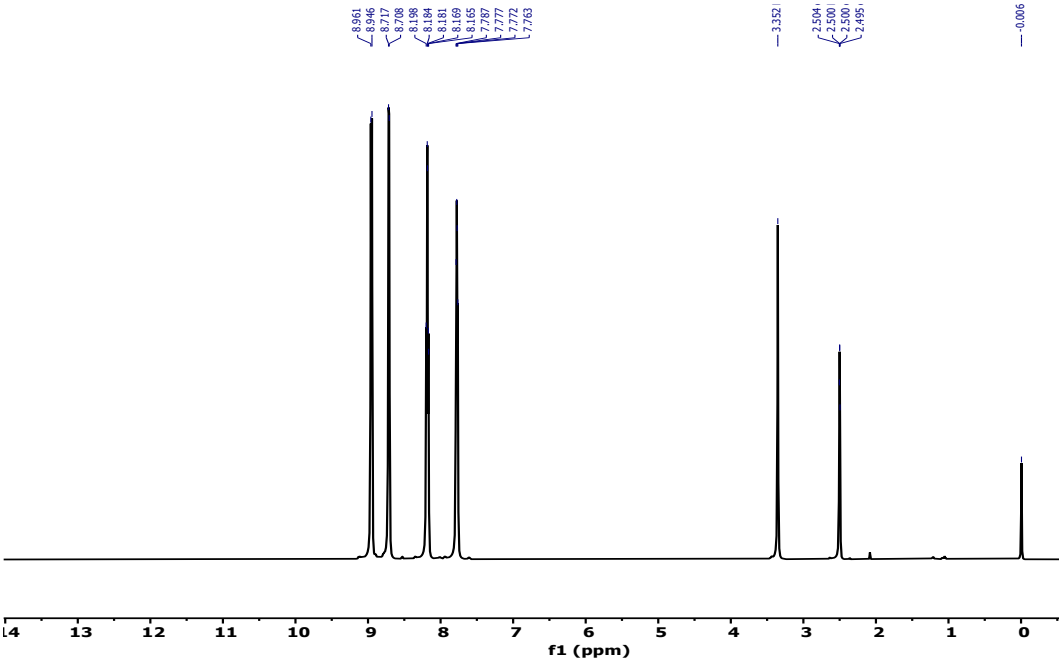

Figure S19. ^{1}H-NMR spectra of complex **Q2** (500 MHz, DMSO-d_6).

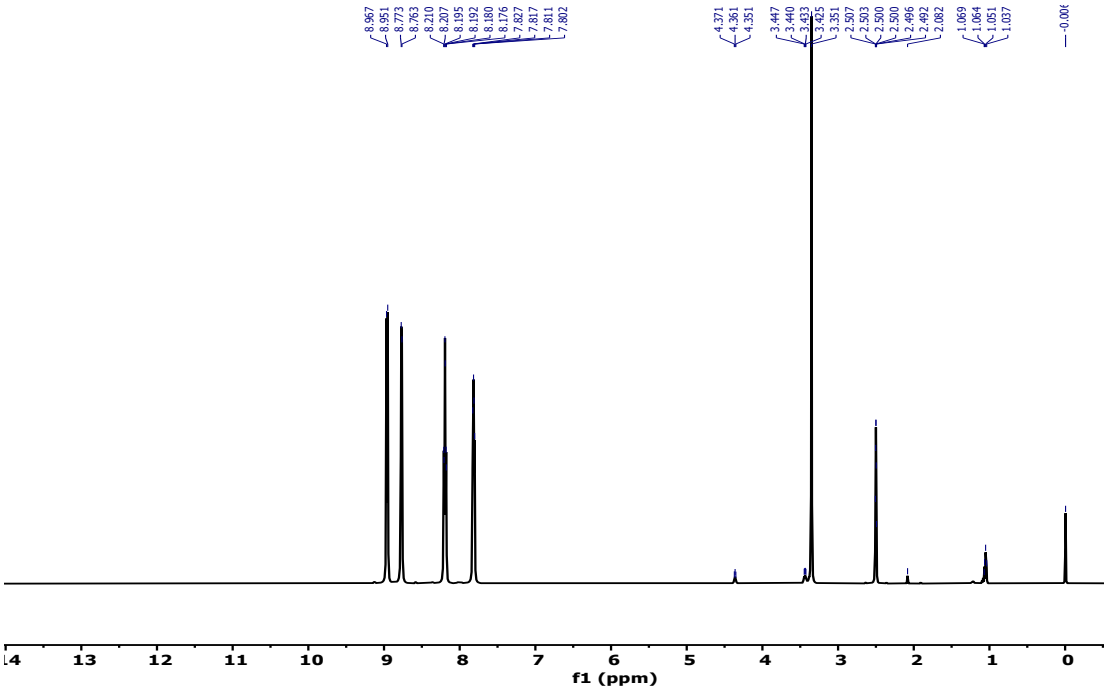

Figure S20. ^{1}H-NMR spectra of complex **Q3** (500 MHz, DMSO-d_6).

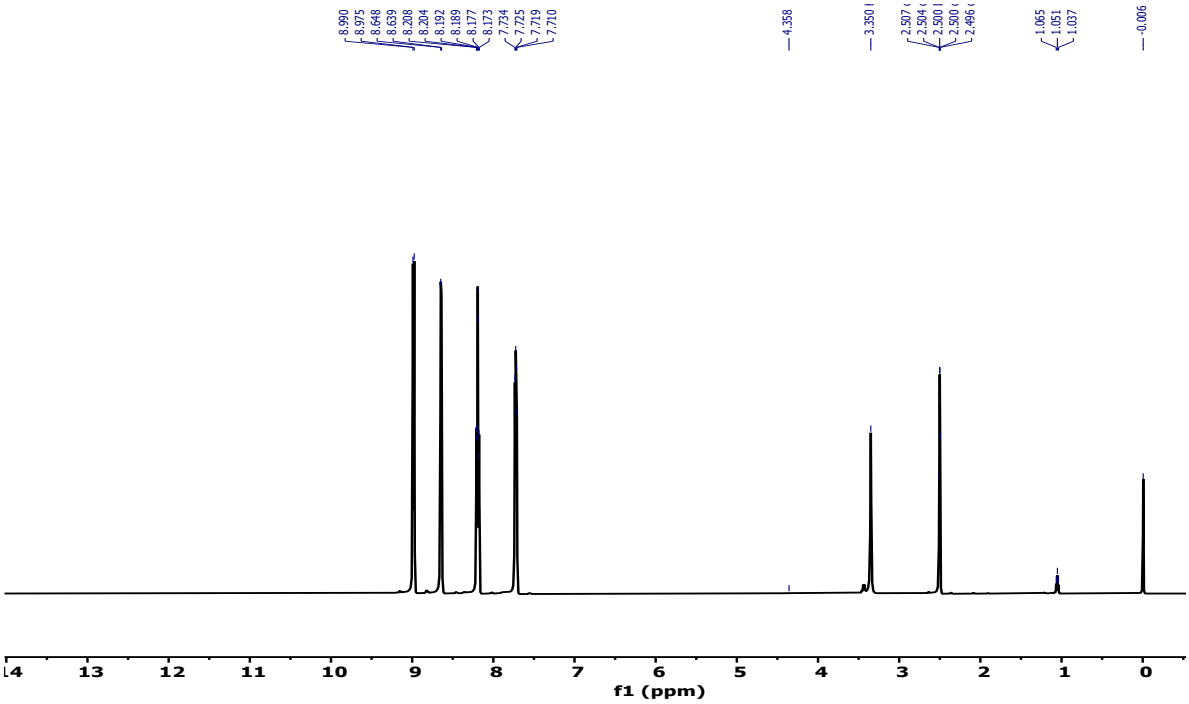

Figure S21. ^{1}H-NMR spectra of complex **Q4** (500 MHz, DMSO-d_6).

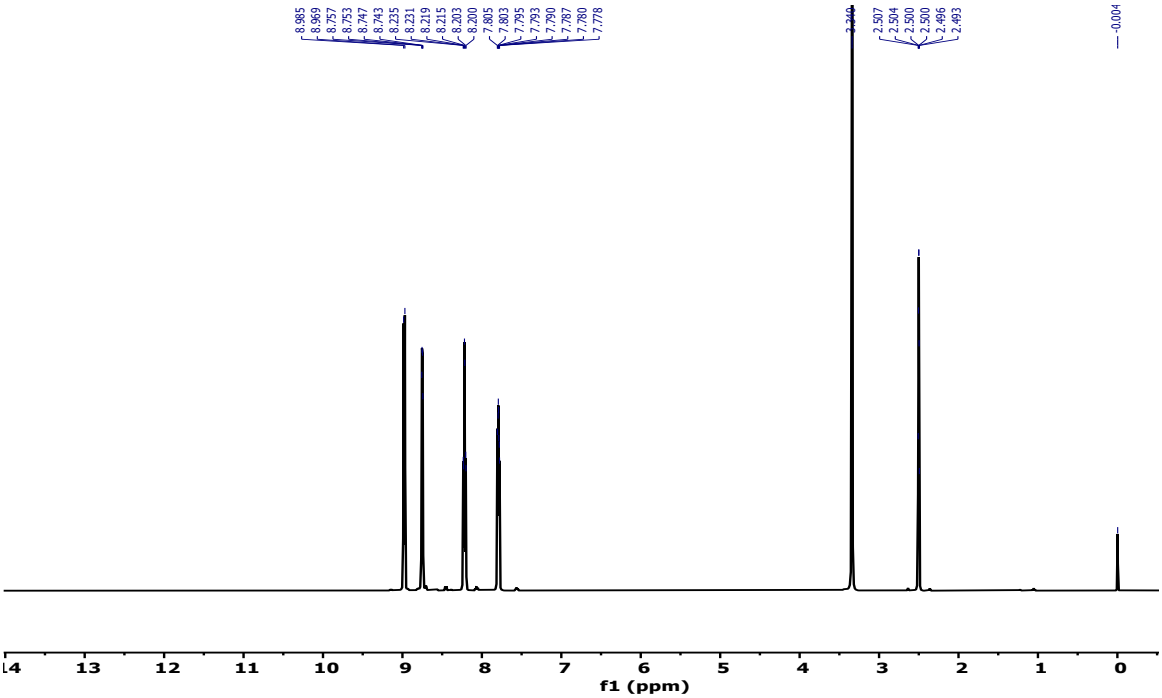

Figure S22. ^{1}H-NMR spectra of complex **Q5** (500 MHz, DMSO-d_6).

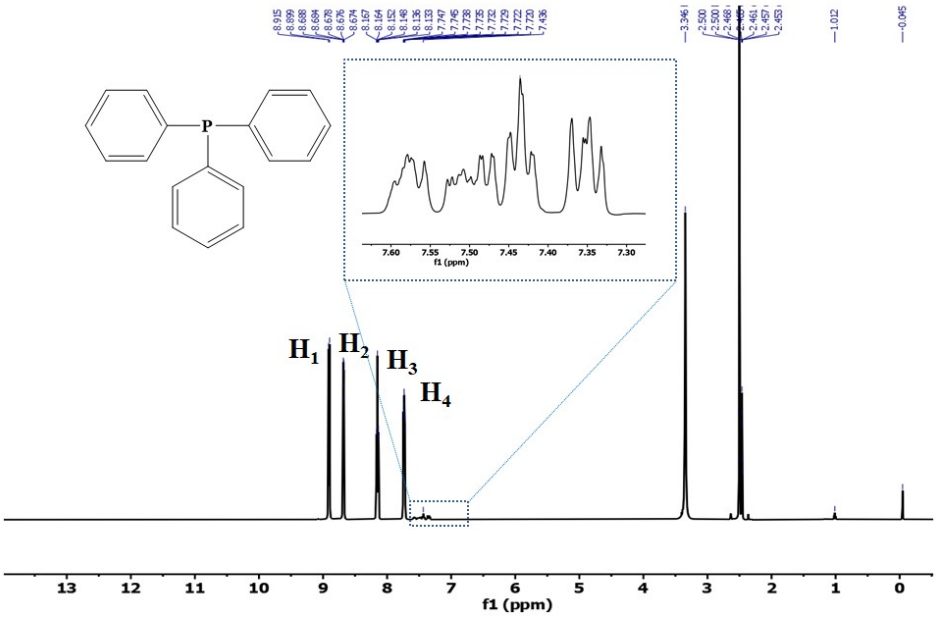

Figure S23. ^{1}H-NMR spectra of complex **Q6** (500 MHz, DMSO-d_6).

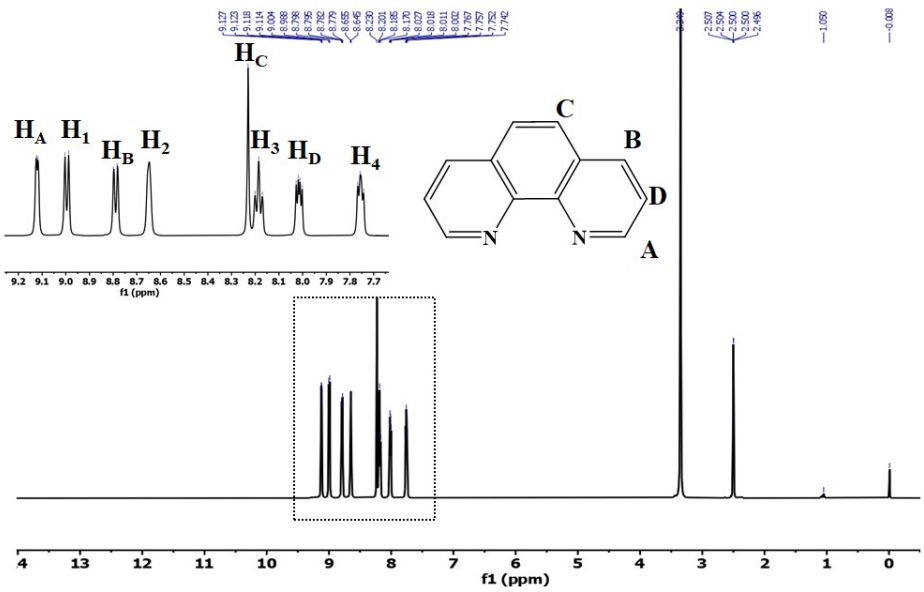

Figure S24. ^{1}H-NMR spectra of complex **Q7** (500 MHz, DMSO-d_6).

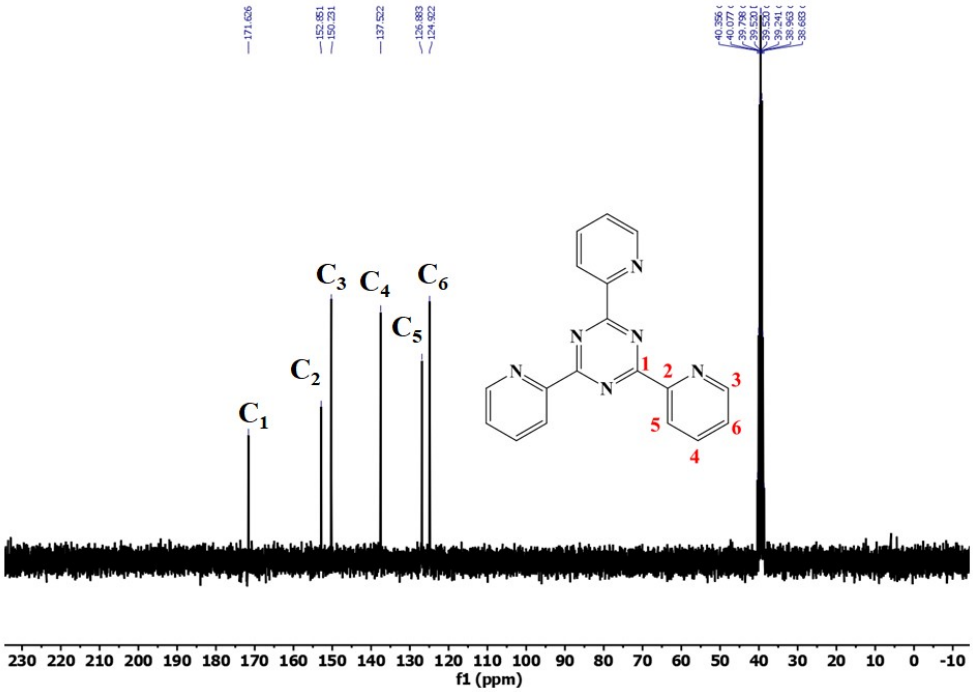

Figure S25. ^{13}C-NMR spectra of ***TPT*** ligand (125 MHz, DMSO-d_6).

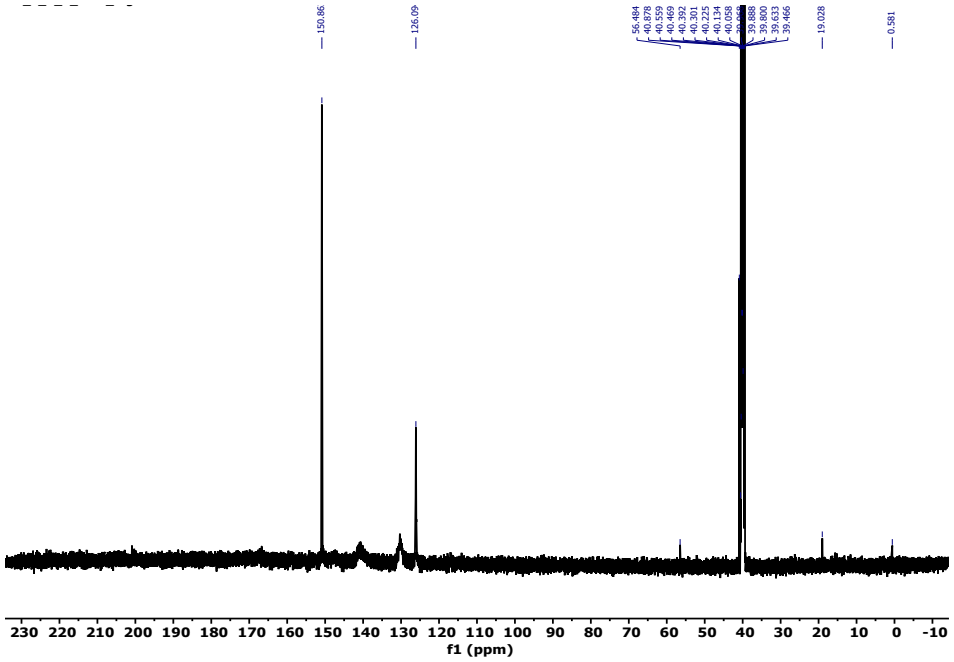

Figure S26. ^{13}C-NMR spectra of complex **Q1** (125 MHz, DMSO-d_6).

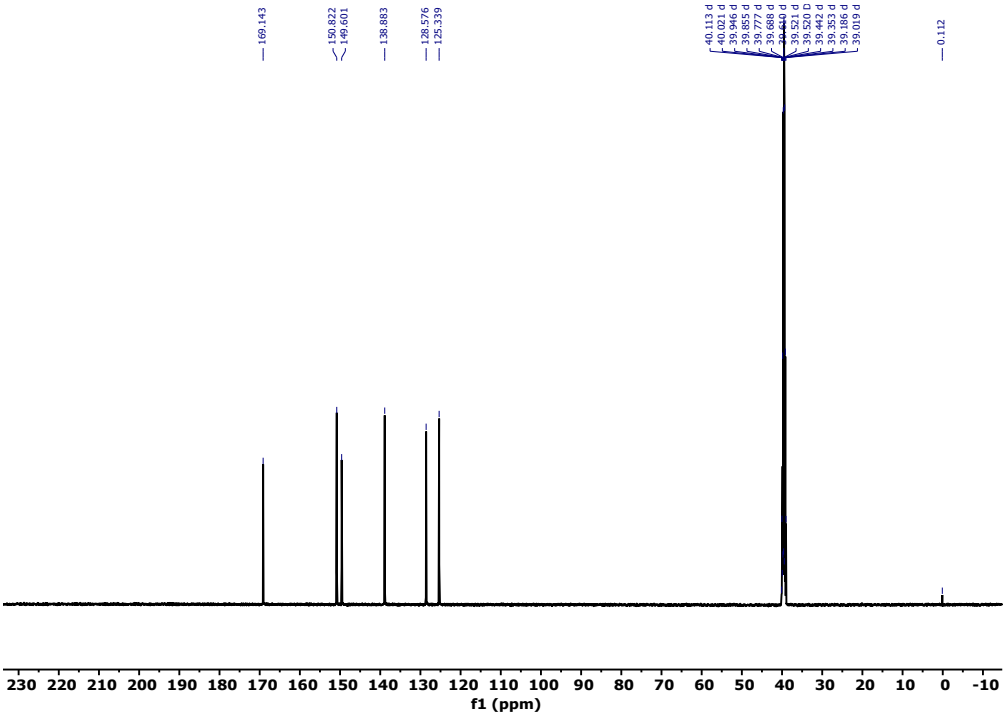

Figure S27. ^{13}C-NMR spectra of complex **Q2** (125 MHz, DMSO-d_6).

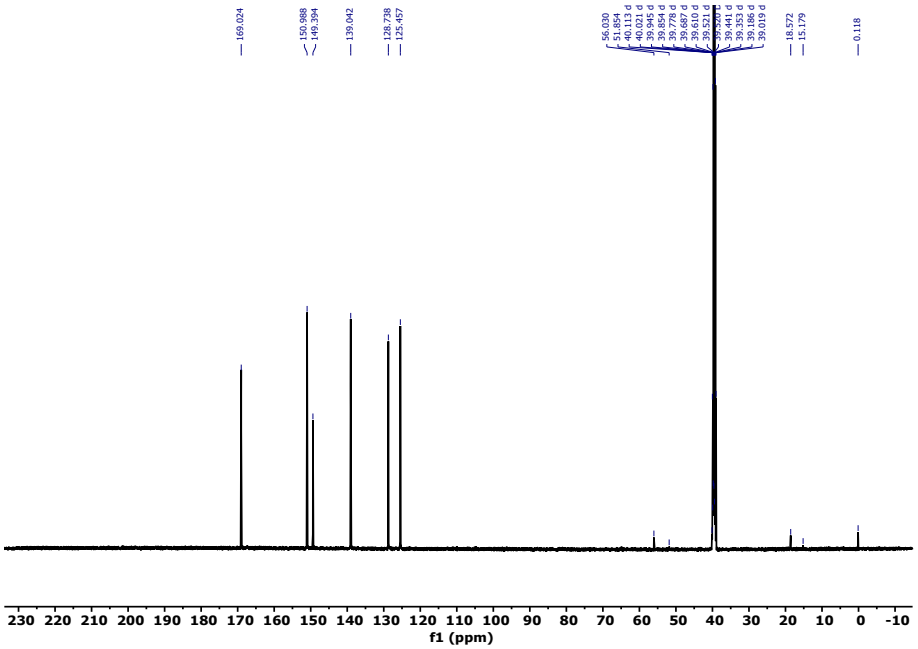

Figure S28. ^{13}C-NMR spectra of complex **Q3** (125 MHz, DMSO-d_6).

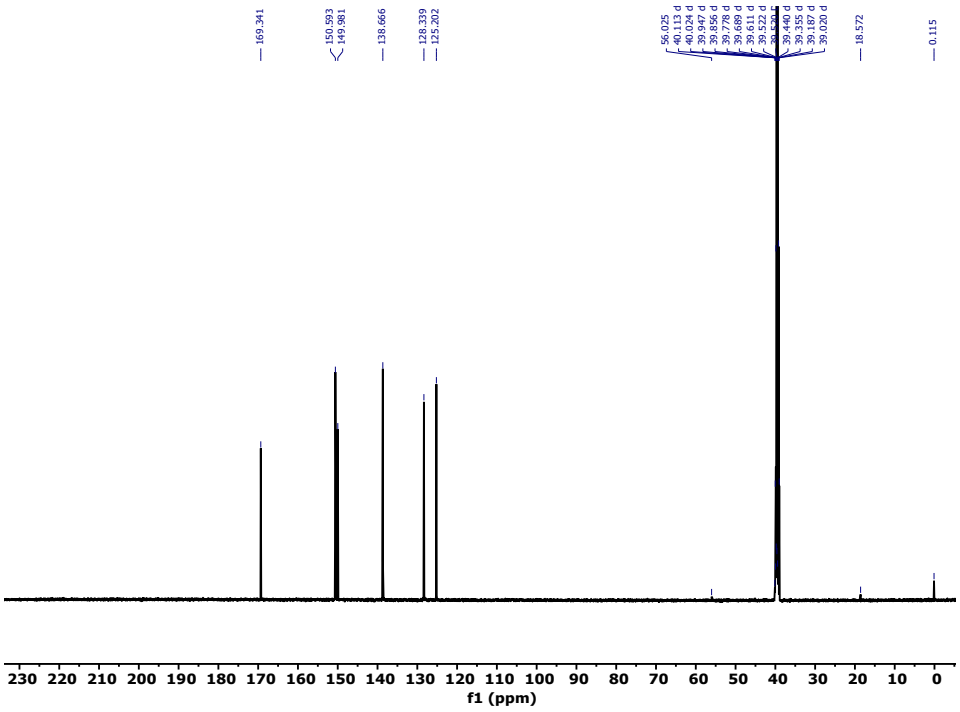

Figure S29. ^{13}C-NMR spectra of complex **Q4** (125 MHz, DMSO-d_6).

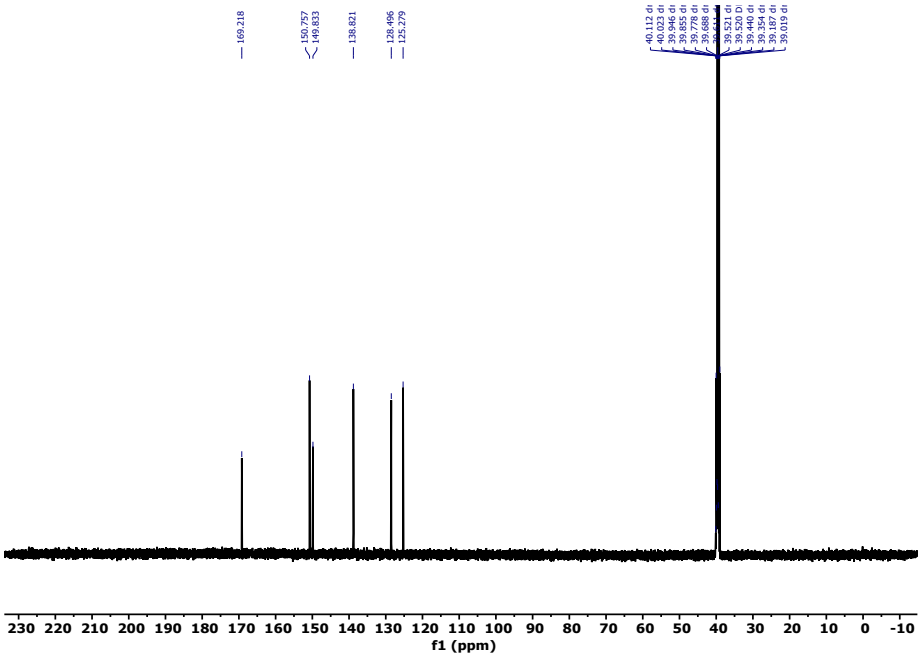

Figure S30. ^{13}C-NMR spectra of complex **Q5** (125 MHz, DMSO-d_6).

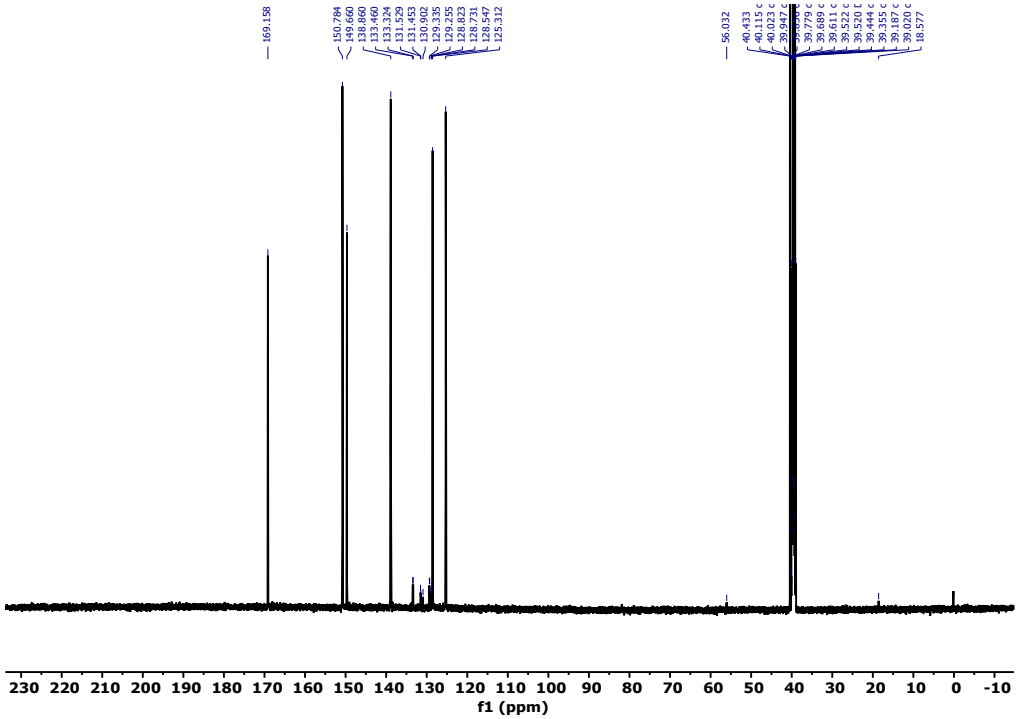

Figure S31. ^{13}C-NMR spectra of complex **Q6** (125 MHz, DMSO-d_6).

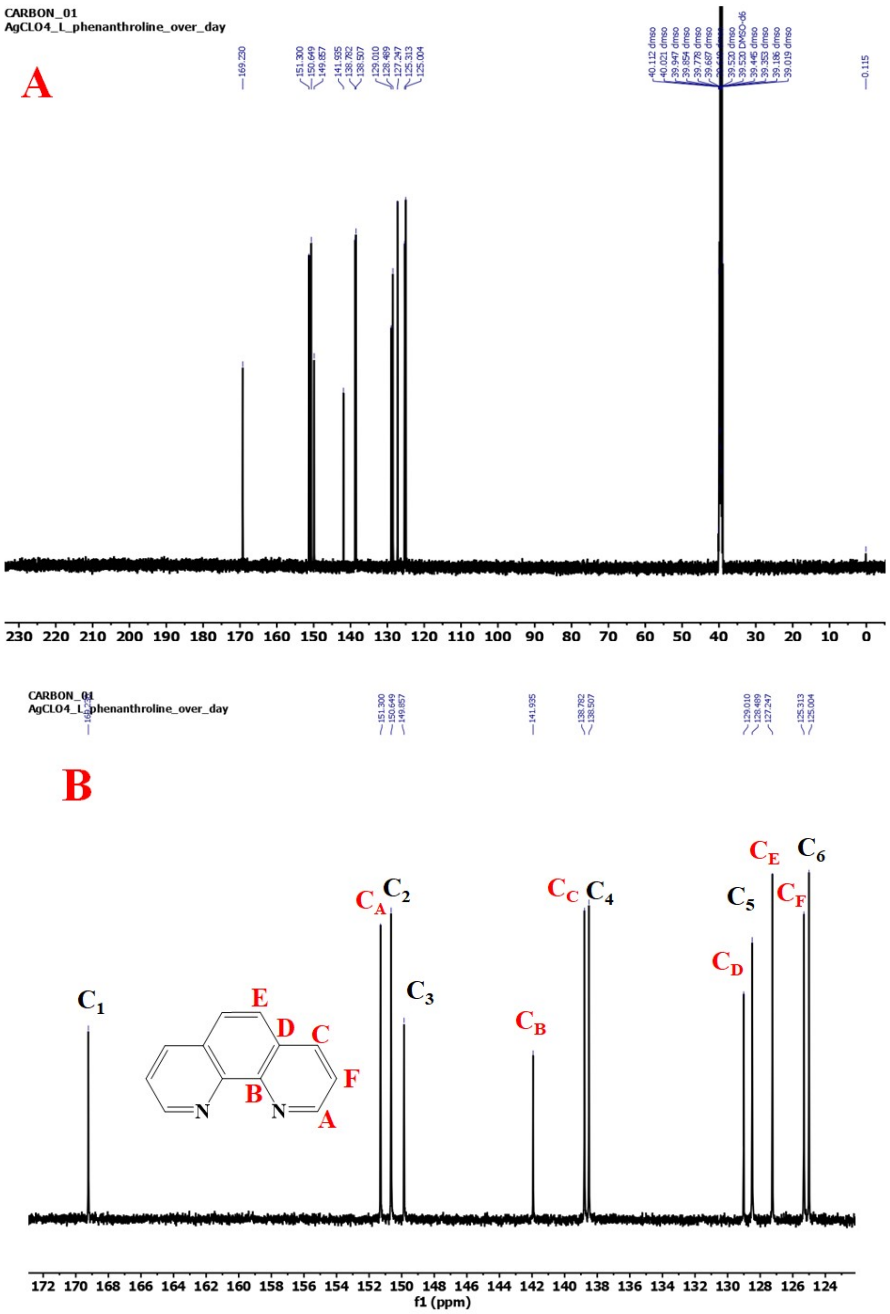

Figure S32. ^{13}C-NMR spectra of complex **Q7** (125 MHz, DMSO-d_6) A) whole spectrum and B) zoomed spectrum.

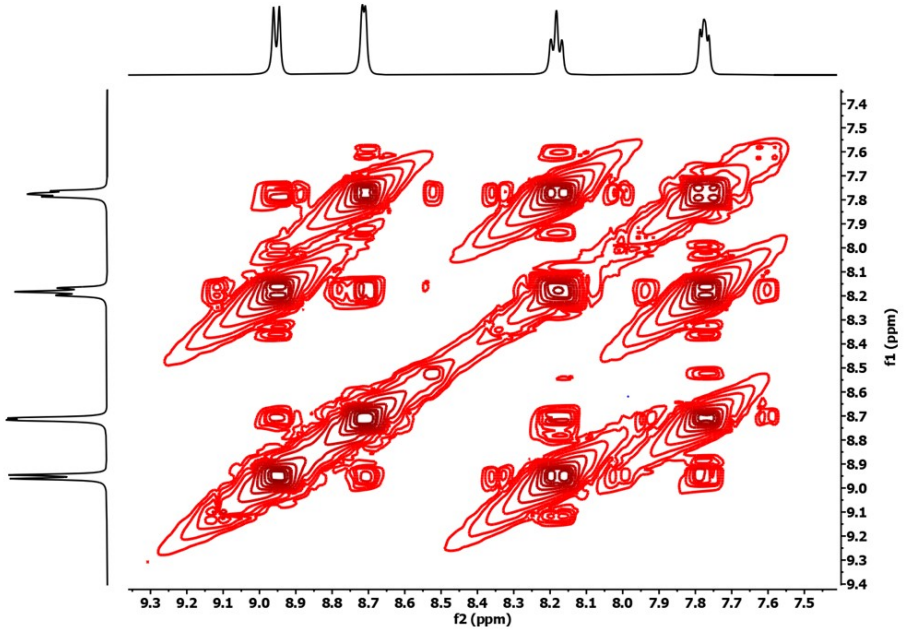

Figure S33. ^{1}H-^{1}H COSY spectrum of complex **Q2** (500 MHz, DMSO-d_6).

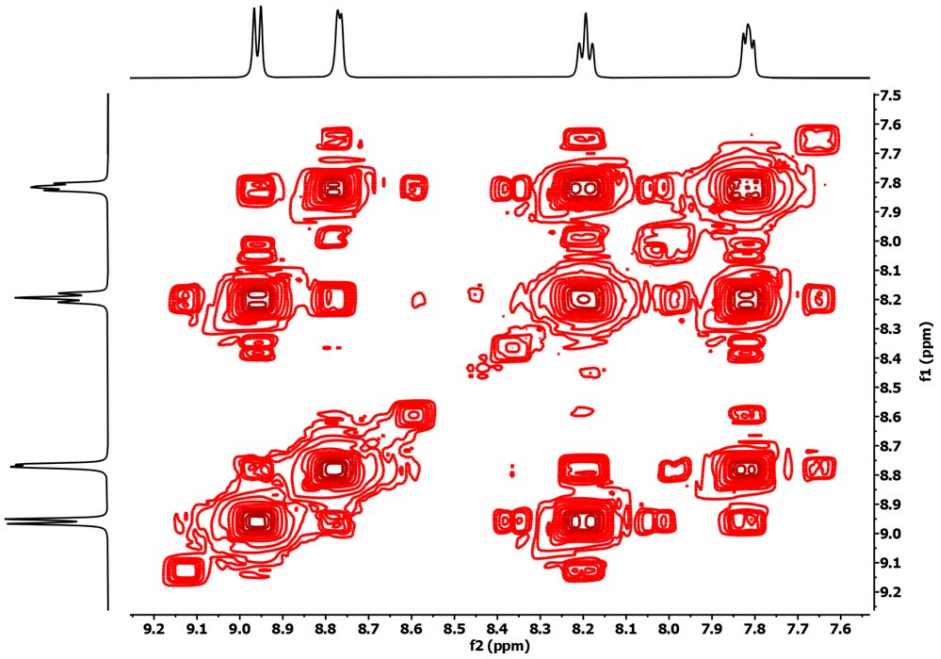

Figure S34. ^{1}H-^{1}H COSY spectrum of complex **Q3** (500 MHz, DMSO-d_6).

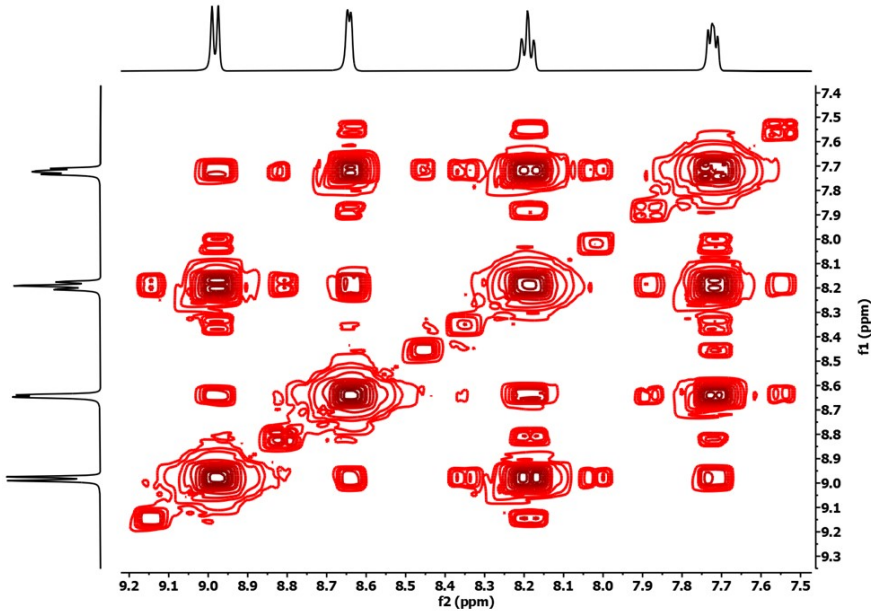

Figure S35. ^{1}H-^{1}H COSY spectrum of complex **Q4** (500 MHz, DMSO-d_6).

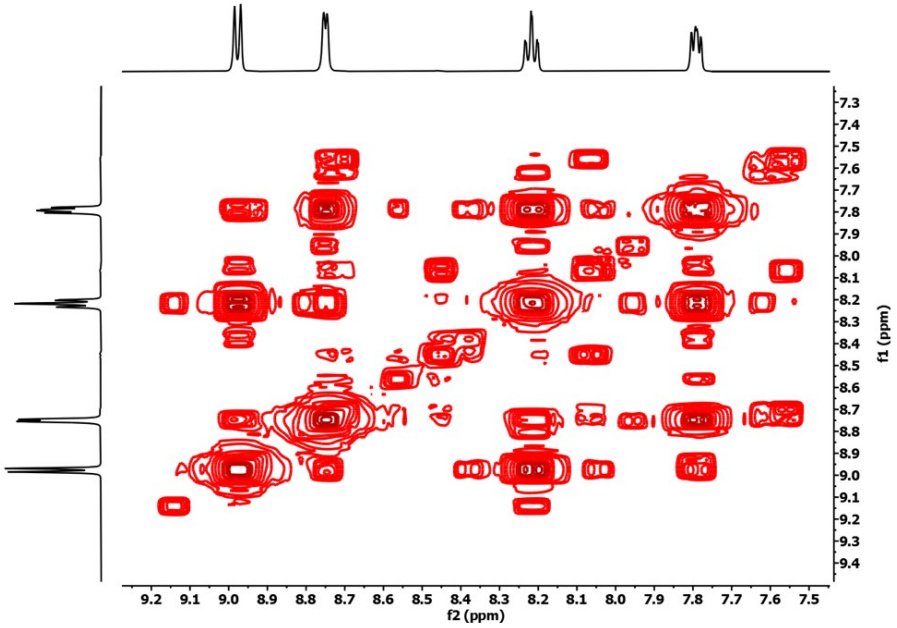

Figure S36. ^{1}H-^{1}H COSY spectrum of complex **Q5** (500 MHz, DMSO-d_6).

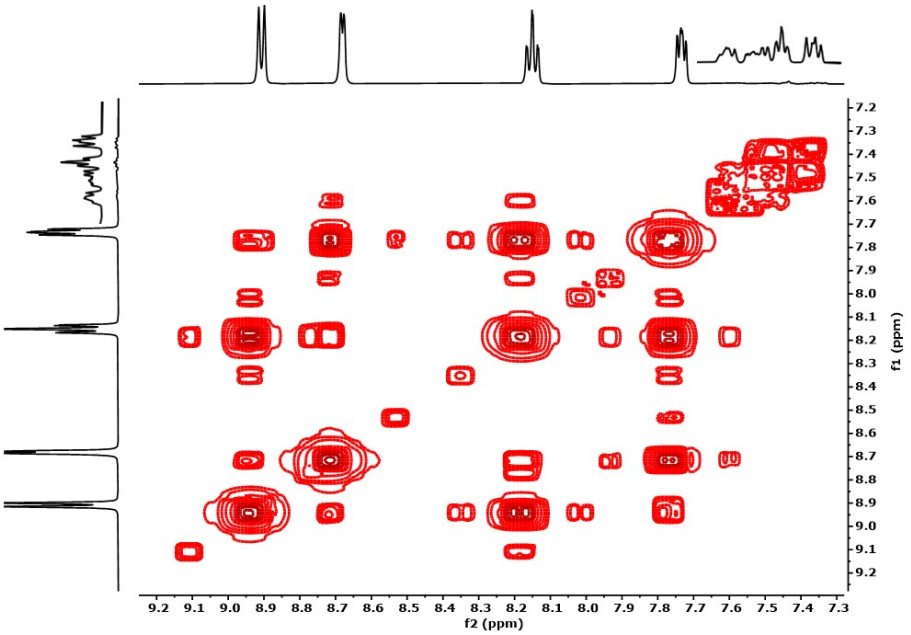

Figure S37. ^{1}H-^{1}H COSY spectrum of complex **Q6** (500 MHz, DMSO-d_6).

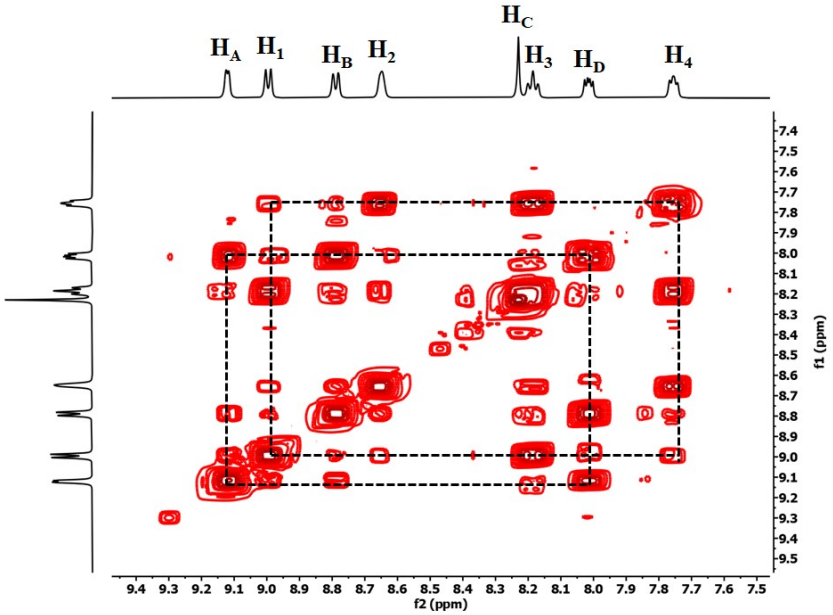

Figure S38. ^{1}H-^{1}H COSY spectrum of complex **Q7** (500 MHz, DMSO-d_6).

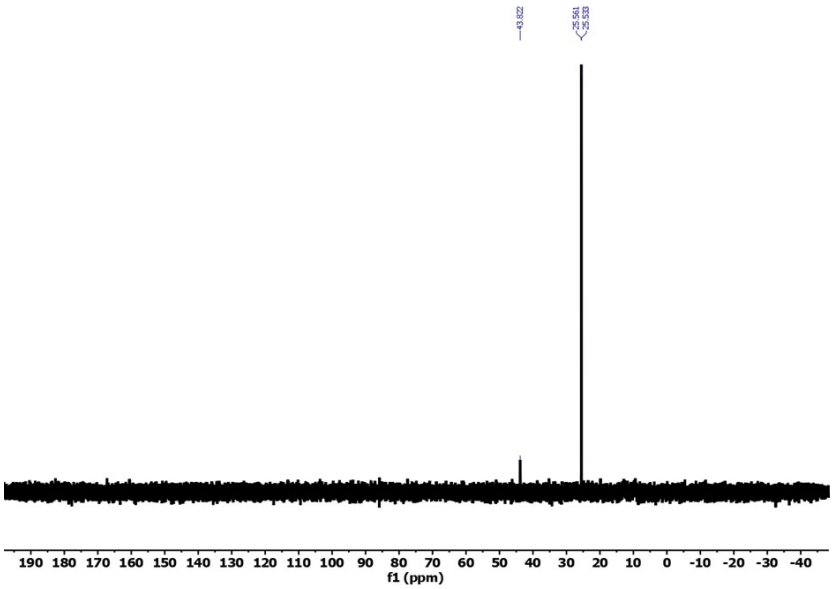

Figure S39. ^{31}P-NMR spectrum of complex **Q6** (202.5 MHz, DMSO-d_6).

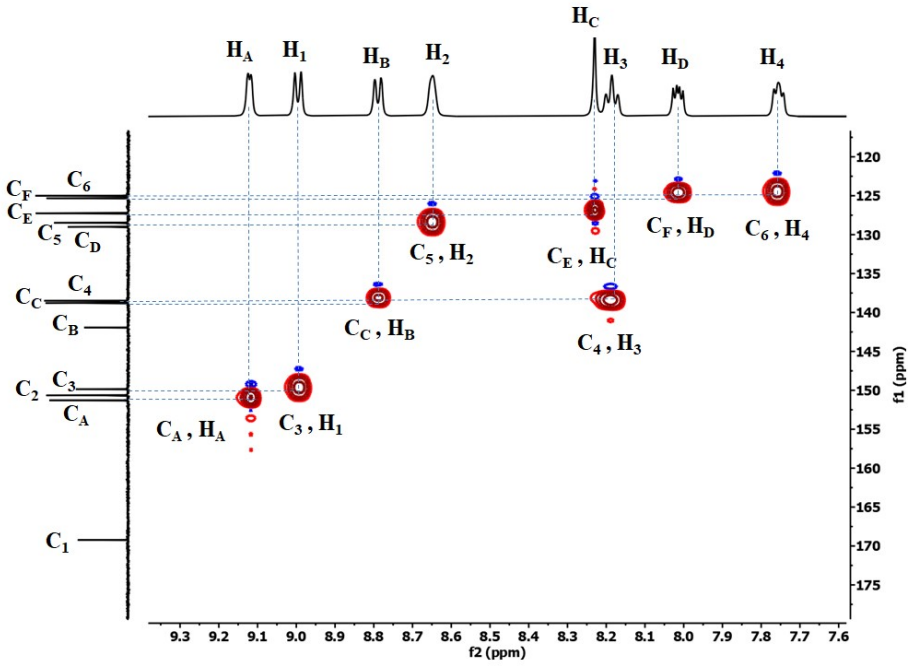

Figure S40. ^{1}H-^{13}C HSQCAD spectrum of complex **Q7** (500 MHz, DMSO-d_6).

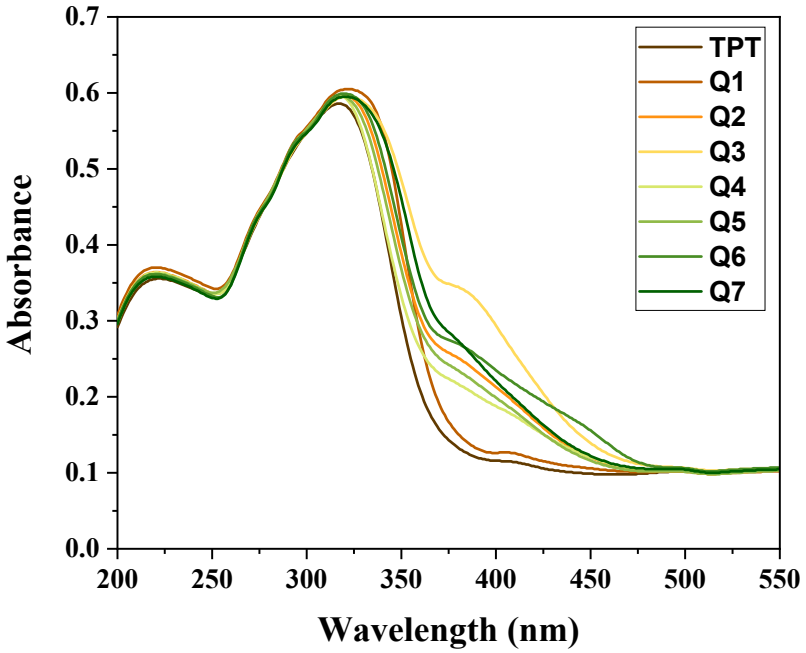

Figure S41. Electronic spectra of ***TPT*** and complexes **Q1-Q7**.

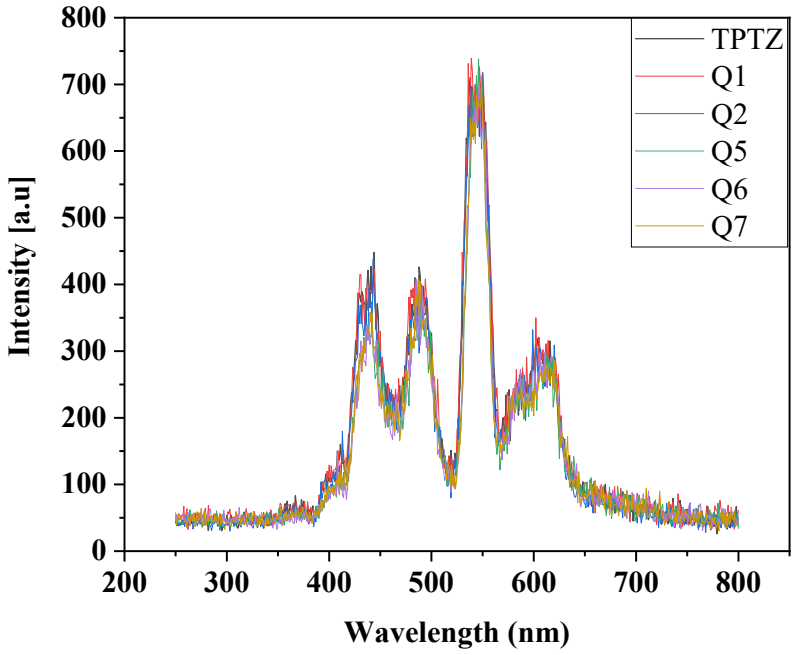

Figure S42. Fluorescence spectra of ***TPT*** [4] and complexes **Q1-Q7**.

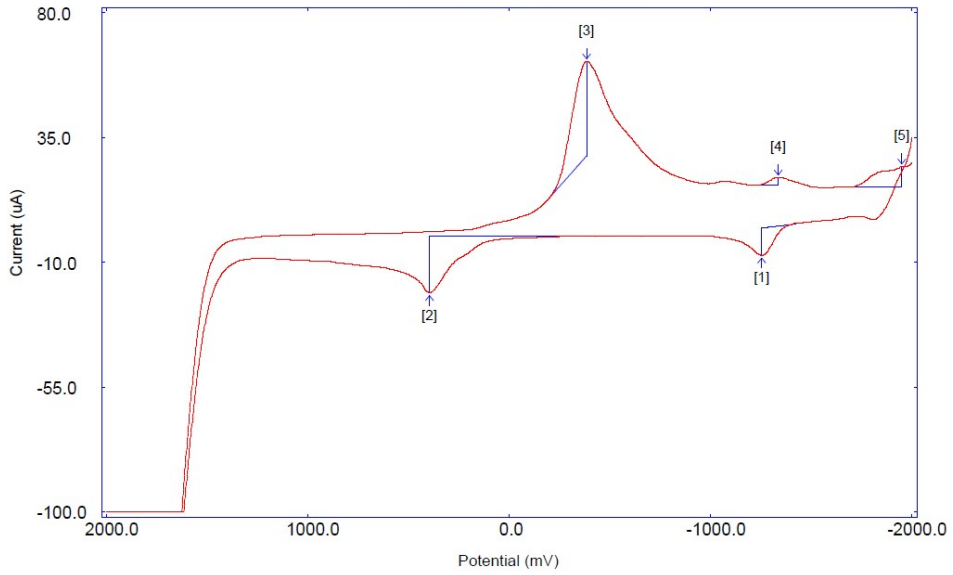

Figure S43. Cyclic voltammogram in DMSO solution with 0.1 M tetrabutylammonium perchlorate (TBAP), scan rate 50 mVs^{-1} for 10^{-3} M of **Q5**

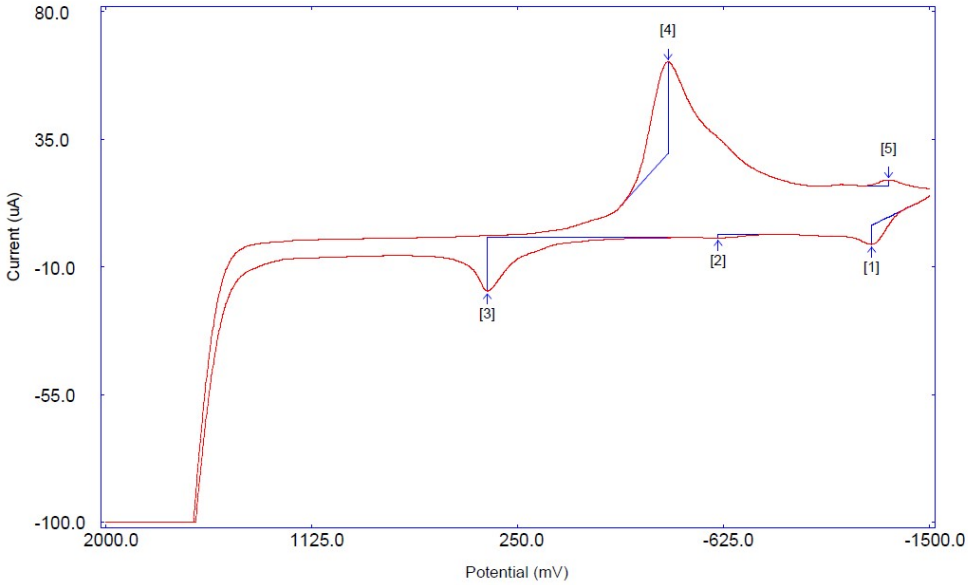

Figure S44. Cyclic voltammogram in DMSO solution with 0.1 M tetrabutylammonium perchlorate (TBAP), scan rate 50 mVs^{-1} for 10^{-3} M of **Q6**

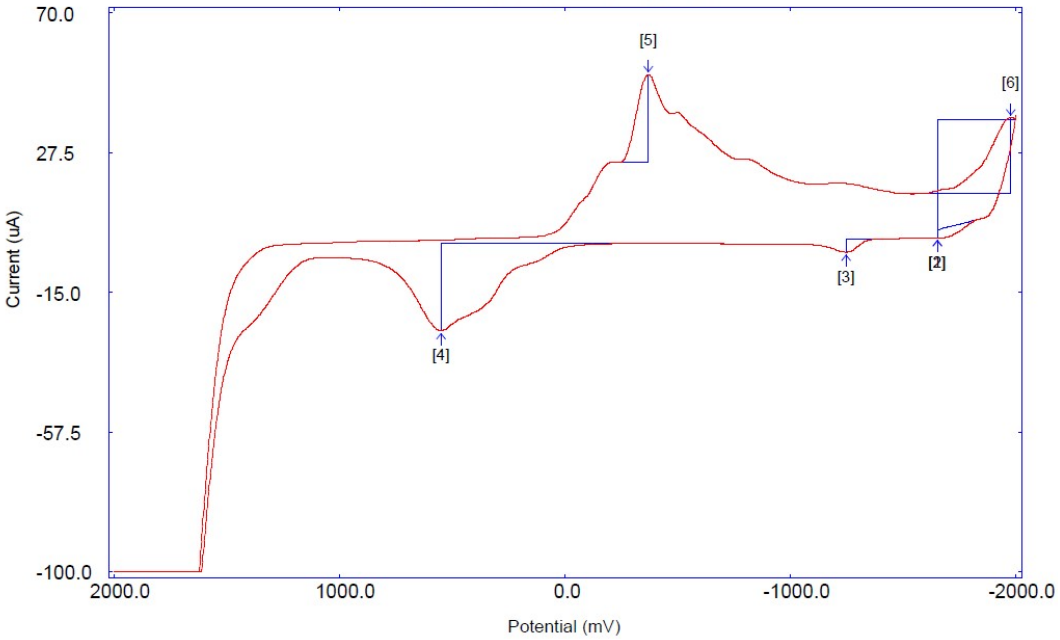

Figure S45. Cyclic voltammogram in DMSO solution with 0.1 M tetrabutylammonium perchlorate (TBAP), scan rate 50 mVs^{-1} for 10^{-3} M of **Q7**

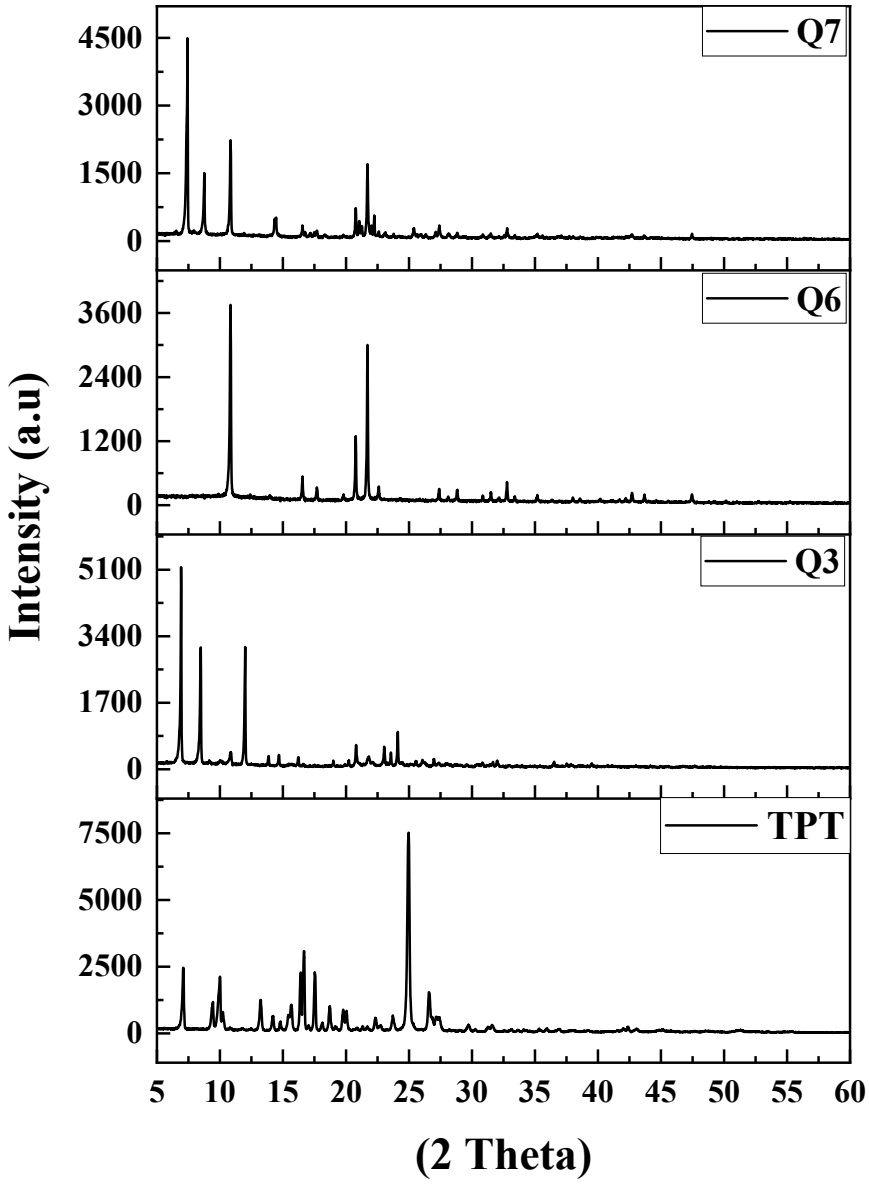

Figure S46. XRD pattern of ***TPT***[4] and complexes **Q3**, **Q6** and **Q7** in powder form at 298 K.

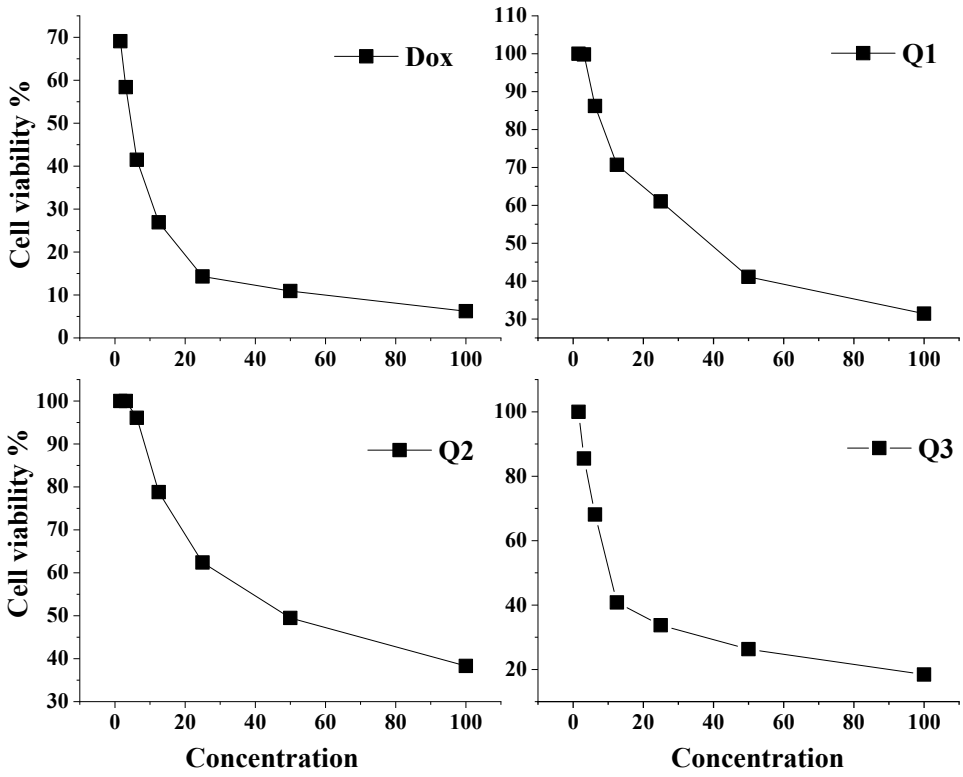
Dox
Q1
Q2
Q3
Cell viability %
Cell viability %
Concentration
Concentration

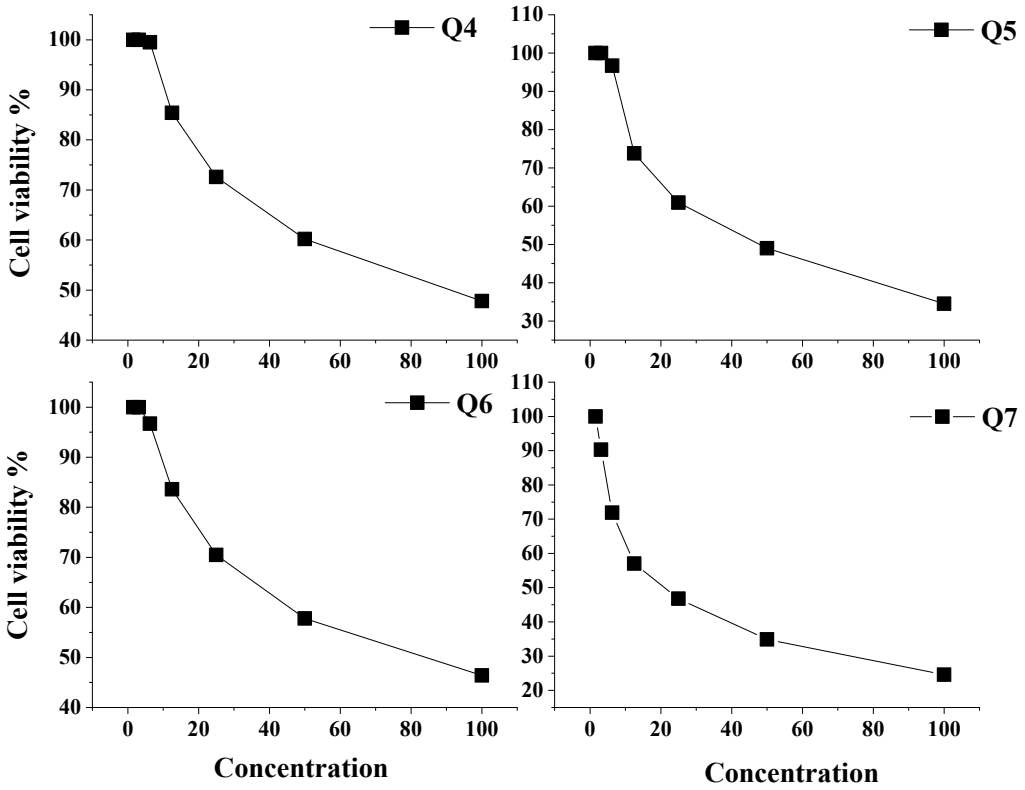

Figure S47. Cytotoxic activity against MCF-7 cell line.

Table S1: ^{1}H-NMR chemical shifts of *TPT* ligand and its metal complexes.

	H^{1}	H^{2}	H^{3}	H^{4}
TPT	8.869	8.707	8.0906	7.6712
Q1	9.0445	8.942	8.374	8.003
Q2	8.9535	8.7125	8.181	7.7748
Q3	8.959	8.768	8.194	7.814
Q4	8.9825	8.6435	8.1905	7.722
Q5	8.977	8.75	8.2172	7.7914
Q6	8.907	8.678	8.149	7.7335
Q7	8.996	8.65	8.185	7.7545

Table S2: ^{13}C-NMR chemical shifts of *TPT* ligand and its metal complexes.

	C_1	C_2	C_3	C_4	C_5	C_6
TPT	171.626	152.851	150.231	137.522	126.883	124.922
Q1	---	---	150.415	140.27	129.836	125.647

Q2	169.143	150.822	149.601	138.883	128.576	125.339
Q3	169.024	150.988	149.394	139.042	128.738	125.457
Q4	169.341	150.593	149.981	138.666	128.339	125.202
Q5	169.218	150.757	149.833	138.821	128.496	125.279
Q6	169.158	150.784	149.660	138.860	128.547	125.312
Q7	169.230	150.649	149.857	138.507	128.489	125.004

Table S3: The average crystallite size of *TPT* and its complexes estimated from XRD pattern

Compound	2θ (°)	d value (A°)	Relative intensity (%)	Full width at Half maximum (FWHM)[a]	Average crystallite size (nm)
TPT	24.95494	3.568	100	0.21709	6.832
Q3	6.91092	12.780	100	0.09669	15.005
Q6	10.82548	8.166	100	0.12338	11.789
Q7	7.39252	11.949	100	0.14867	9.761

[a] The maximum diffraction patterns according to the highest value of intensity

Table S4. Crystal data and structure refinement for complexes **Q6**.

Compounds	**Q6 (Deposition Number 1509097)**
Empirical formula	$C_{56}H_{48}AgClN_6O_5P_2$
Formula weight	1090.26
Temperature	100(2) K
Wavelength	1.54178 Å
Crystal system	Triclinic
Space group	P-1
Unit cell dimensions	
a (Å)	9.9899(11) Å
b (Å)	14.6866(16) Å
c (Å)	17.880(2) Å
α (°)	88.277(5)°
β (°)	77.431(4)°
γ (°)	78.288(5)°
Volume	2506.8(5) $Å^3$
Z	2
Density (calculated)	1.444 Mg/m^3
Absorption coefficient	4.773 mm^{-1}
F(000)	1120
Crystal size	0.410 x 0.360 x 0.240 mm^3

Theta range for data collection	2.532 to 68.414°.
Index ranges	-11<=h<=12, -14<=k<=17, -21<=l<=21
Reflections collected	21420
Independent reflections	9013 [R(int) = 0.0328]
Completeness to theta = 67.679°	98.40%
Absorption correction	Semi-empirical from equivalents
Refinement method	Full-matrix least-squares on F2
Data / restraints / parameters	9013 / 736 / 693
Goodness-of-fit on F2	1.075
Final R indices [I>2sigma(I)]	R1 = 0.0336, wR2 = 0.0864
R indices (all data)	R1 = 0.0342, wR2 = 0.0870
Extinction coefficient	n/a
Largest diff. peak and hole	1.05 d -0.665 e.Å^{-3}

Table S5. Selected bond lengths (Å) for Q6

Ag(1)-N(3)	2.4197(18)	C(22)-C(23)	1.388(4)	C(71)-C(76)	1.403(3)
Ag(1)-P(2)	2.4715(6)	C(22)-H(22)	0.95	C(72)-C(73)	1.397(4)
Ag(1)-P(1)	2.4757(6)	C(23)-C(24)	1.375(4)	C(72)-H(72)	0.95
Ag(1)-N(2)	2.5719(19)	C(23)-H(23)	0.95	C(73)-C(74)	1.382(4)
Ag(1)-N(1)	2.711(2)	C(24)-C(25)	1.385(4)	C(73)-H(73)	0.95
N(1)-C(1)	1.334(3)	C(24)-H(24)	0.95	C(74)-C(75)	1.380(4)
N(1)-C(5)	1.343(3)	C(25)-C(26)	1.391(4)	C(74)-H(74)	0.95
C(1)-C(2)	1.389(4)	C(25)-H(25)	0.95	C(75)-C(76)	1.387(4)
C(1)-H(1)	0.95	C(26)-H(26)	0.95	C(75)-H(75)	0.95
C(2)-C(3)	1.390(4)	C(31)-C(36)	1.397(3)	C(76)-H(76)	0.95
C(2)-H(2)	0.95	C(31)-C(32)	1.398(3)	Cl(1S)-O(1S)	1.432(2)
C(3)-C(4)	1.386(4)	C(33)-H(33)	0.95	Cl(1S)-O(2S)	1.433(2)
C(3)-H(3)	0.95	C(34)-C(35)	1.389(4)	Cl(1S)-O(3S)	1.443(2)
C(4)-C(5)	1.391(3)	C(34)-H(34)	0.95	Cl(1S)-O(4S)	1.448(3)
C(4)-H(4)	0.95	C(35)-C(36)	1.389(3)	Cl(1U)-O(2U)	1.416(14)
C(5)-C(6)	1.488(3)	C(35)-H(35)	0.95	N(4)-C(13)	1.430(14)
C(6)-N(4)	1.335(3)	C(36)-H(36)	0.95	Cl(1U)-O(3U)	1.450(12)
C(6)-N(3)	1.343(3)	C(41)-C(46)	1.391(3)	Cl(1U)-O(4U)	1.466(12)
N(2)-C(11)	1.340(3)	C(41)-C(42)	1.392(3)	O(1TA)-C(1TA)	1.360(5)
N(2)-C(7)	1.341(3)	C(42)-C(43)	1.394(3)	O(1TA)-H(1TA)	0.854(15)
C(7)-C(8)	1.386(3)	C(42)-H(42)	0.95	C(1TA)-C(2TA)	1.514(6)
C(7)-H(7)	0.95	C(43)-C(44)	1.387(4)	C(1TA)-H(1T1)	0.99
C(8)-C(9)	1.382(4)	C(43)-H(43)	0.95	C(2TA)-H(2T3)	0.98
C(8)-H(8)	0.95	C(44)-C(45)	1.383(4)	O(1TB)-C(1TB)	1.452(16)
C(9)-C(10)	1.393(3)	C(44)-H(44)	0.95	O(1TB)-H(1TB)	0.844(15)
C(9)-H(9)	0.95	C(45)-C(46)	1.390(3)	C(1TB)-C(2TB)	1.457(17)
C(10)-C(11)	1.392(3)	C(45)-H(45)	0.95	C(1TB)-H(1T3)	0.99
C(10)-H(10)	0.95	C(46)-H(46)	0.95	C(1TB)-H(1T4)	0.99
C(11)-C(12)	1.488(3)	P(2)-C(61)	1.828(2)	C(2TB)-H(2T4)	0.98
C(12)-N(5)	1.335(3)	P(2)-C(71)	1.831(2)	C(2TB)-H(2T5)	0.98
C(12)-N(3)	1.344(3)	P(2)-C(51)	1.836(2)	C(2TB)-H(2T6)	0.98
C(14)-N(6B)	1.34(3)	C(51)-C(52)	1.390(3)	O(1TC)-C(1TC)	1.411(19)
C(14)-N(6A)	1.345(14)	C(51)-C(56)	1.398(3)	O(1TC)-H(1TC)	0.845(16)

C(14)-C(15B)	1.38(3)	C(52)-C(53)	1.390(4)	C(1TC)-C(2TC)	1.479(19)
C(14)-C(15A)	1.39(2)	C(52)-H(52)	0.95	C(1TC)-H(1T5)	0.99
C(15A)-C(16)	1.376(17)	C(53)-C(54)	1.387(4)	C(1TC)-H(1T6)	0.99
C(15A)-H(15A)	0.95	C(53)-H(53)	0.95	C(2TC)-H(2T7)	0.98
C(15B)-C(18)	1.36(3)	C(54)-C(55)	1.389(4)	C(2TC)-H(2T8)	0.98
C(15B)-H(15B)	0.95	C(54)-H(54)	0.95	C(2TC)-H(2T9)	0.98
C(16)-N(6B)	1.38(2)	C(55)-C(56)	1.389(3)	N(5)-C(13)	1.338(3)
C(16)-C(17)	1.382(4)	C(55)-H(55)	0.95	C(13)-C(14)	1.488(3)
C(16)-H(16)	0.95	C(56)-H(56)	0.95	C(32)-C(33)	1.391(3)
C(17)-C(18)	1.379(4)	C(62)-H(62)	0.95	C(32)-H(32)	0.95
C(17)-H(17)	0.95	C(63)-C(64)	1.385(4)	C(33)-C(34)	1.390(4)
C(18)-N(6A)	1.342(14)	C(63)-H(63)	0.95	C(61)-C(62)	1.389(3)
C(18)-H(18)	0.95	C(64)-C(65)	1.390(4)	C(61)-C(66)	1.393(3)
P(1)-C(21)	1.825(2)	C(64)-H(64)	0.95	C(62)-C(63)	1.393(3)
P(1)-C(41)	1.826(2)	C(65)-C(66)	1.392(4)	C(1TA)-H(1T2)	0.99
P(1)-C(31)	1.832(2)	C(65)-H(65)	0.95	C(2TA)-H(2T1)	0.98
C(21)-C(22)	1.393(3)	C(66)-H(66)	0.95	C(2TA)-H(2T2)	0.98
C(21)-C(26)	1.396(3)	C(71)-C(72)	1.382(4)		

Table S6. Selected bond angles (°) for Q6

N(3)-Ag(1)-P(2)	115.80(4)	N(5)-C(12)-C(11)	116.97(19)	C(23)-C(24)-C(25)	119.9(2)
N(3)-Ag(1)-P(1)	122.00(4)	N(3)-C(12)-C(11)	117.91(19)	C(23)-C(24)-H(24)	120.1
P(2)-Ag(1)-P(1)	122.154(19)	C(6)-N(3)-C(12)	114.16(19)	C(25)-C(24)-H(24)	120.1
N(3)-Ag(1)-N(2)	66.06(6)	C(6)-N(3)-Ag(1)	124.14(14)	C(24)-C(25)-C(26)	120.0(3)
P(2)-Ag(1)-N(2)	102.77(4)	C(12)-N(3)-Ag(1)	121.67(14)	C(24)-C(25)-H(25)	120
P(1)-Ag(1)-N(2)	101.99(4)	C(13)-N(4)-C(6)	115.00(19)	C(26)-C(25)-H(25)	120
N(3)-Ag(1)-N(1)	64.63(6)	C(12)-N(5)-C(13)	115.32(19)	C(25)-C(26)-C(21)	120.2(2)
P(2)-Ag(1)-N(1)	100.39(4)	N(4)-C(13)-N(5)	124.8(2)	C(25)-C(26)-H(26)	119.9
P(1)-Ag(1)-N(1)	101.46(4)	N(4)-C(13)-C(14)	117.8(2)	C(21)-C(26)-H(26)	119.9
N(2)-Ag(1)-N(1)	130.62(6)	N(5)-C(13)-C(14)	117.4(2)	C(36)-C(31)-C(32)	119.0(2)
C(1)-N(1)-C(5)	117.0(2)	N(6B)-C(14)-C(15B)	123.6(10)	C(36)-C(31)-P(1)	118.91(17)
C(1)-N(1)-Ag(1)	126.42(16)	N(6A)-C(14)-C(15A)	123.2(6)	C(32)-C(31)-P(1)	121.96(17)
C(5)-N(1)-Ag(1)	113.52(14)	N(6B)-C(14)-C(13)	120.0(13)	C(33)-C(32)-C(31)	120.4(2)
N(1)-C(1)-C(2)	123.3(2)	N(6A)-C(14)-C(13)	117.8(7)	C(33)-C(32)-H(32)	119.8
N(1)-C(1)-H(1)	118.3	C(15B)-C(14)-C(13)	116.3(13)	C(31)-C(32)-H(32)	119.8
C(2)-C(1)-H(1)	118.3	C(15A)-C(14)-C(13)	119.0(9)	C(34)-C(33)-C(32)	120.1(2)
C(1)-C(2)-C(3)	118.7(2)	C(16)-C(15A)-C(14)	116.7(17)	C(34)-C(33)-H(33)	120
C(1)-C(2)-H(2)	120.7	C(16)-C(15A)-H(15A)	121.7	C(32)-C(33)-H(33)	120
C(3)-C(2)-H(2)	120.7	C(14)-C(15A)-H(15A)	121.7	C(35)-C(34)-C(33)	119.7(2)
C(4)-C(3)-C(2)	119.1(2)	C(18)-C(15B)-C(14)	115(2)	C(35)-C(34)-H(34)	120.1
C(4)-C(3)-H(3)	120.5	C(18)-C(15B)-H(15B)	122.4	C(33)-C(34)-H(34)	120.1
C(2)-C(3)-H(3)	120.5	C(14)-C(15B)-H(15B)	122.4	C(36)-C(35)-C(34)	120.4(2)
C(3)-C(4)-C(5)	117.7(2)	C(15A)-C(16)-C(17)	121.2(10)	C(36)-C(35)-H(35)	119.8
C(3)-C(4)-H(4)	121.1	N(6B)-C(16)-C(17)	118.8(15)	C(34)-C(35)-H(35)	119.8
C(5)-C(4)-H(4)	121.1	C(15A)-C(16)-H(16)	119.4	C(35)-C(36)-C(31)	120.3(2)
N(1)-C(5)-C(4)	124.1(2)	C(17)-C(16)-H(16)	119.4	C(35)-C(36)-H(36)	119.9
N(1)-C(5)-C(6)	117.1(2)	C(18)-C(17)-C(16)	118.1(2)	C(31)-C(36)-H(36)	119.9
C(4)-C(5)-C(6)	118.7(2)	C(18)-C(17)-H(17)	121	C(46)-C(41)-C(42)	119.7(2)
N(4)-C(6)-N(3)	125.5(2)	C(16)-C(17)-H(17)	121	C(46)-C(41)-P(1)	116.10(17)
N(4)-C(6)-C(5)	116.5(2)	N(6A)-C(18)-C(17)	122.3(7)	C(42)-C(41)-P(1)	124.14(17)
N(3)-C(6)-C(5)	117.94(19)	C(15B)-C(18)-C(17)	124.1(13)	C(41)-C(42)-C(43)	119.7(2)

C(11)-N(2)-C(7)	117.40(19)	N(6A)-C(18)-H(18)	118.9	C(41)-C(42)-H(42)	120.2
C(11)-N(2)-Ag(1)	117.08(14)	C(17)-C(18)-H(18)	118.9	C(43)-C(42)-H(42)	120.2
C(7)-N(2)-Ag(1)	124.79(15)	C(18)-N(6A)-C(14)	118.4(12)	C(44)-C(43)-C(42)	120.2(2)
N(2)-C(7)-C(8)	123.1(2)	C(14)-N(6B)-C(16)	120(3)	C(44)-C(43)-H(43)	119.9
N(2)-C(7)-H(7)	118.4	C(21)-P(1)-C(41)	105.07(10)	C(42)-C(43)-H(43)	119.9
C(8)-C(7)-H(7)	118.4	C(21)-P(1)-C(31)	103.00(10)	C(45)-C(44)-C(43)	120.2(2)
C(9)-C(8)-C(7)	119.0(2)	C(41)-P(1)-C(31)	102.36(10)	C(45)-C(44)-H(44)	119.9
C(9)-C(8)-H(8)	120.5	C(21)-P(1)-Ag(1)	111.65(7)	C(43)-C(44)-H(44)	119.9
C(7)-C(8)-H(8)	120.5	C(41)-P(1)-Ag(1)	117.69(7)	C(44)-C(45)-C(46)	119.8(2)
C(8)-C(9)-C(10)	118.9(2)	C(31)-P(1)-Ag(1)	115.47(7)	C(44)-C(45)-H(45)	120.1
C(8)-C(9)-H(9)	120.6	C(22)-C(21)-C(26)	119.2(2)	C(46)-C(45)-H(45)	120.1
C(10)-C(9)-H(9)	120.6	C(22)-C(21)-P(1)	122.19(18)	C(45)-C(46)-C(41)	120.4(2)
C(11)-C(10)-C(9)	118.1(2)	C(26)-C(21)-P(1)	118.31(18)	C(45)-C(46)-H(46)	119.8
C(11)-C(10)-H(10)	120.9	C(23)-C(22)-C(21)	119.9(2)	C(41)-C(46)-H(46)	119.8
C(9)-C(10)-H(10)	120.9	C(23)-C(22)-H(22)	120.1	C(61)-P(2)-C(71)	102.54(10)
N(2)-C(11)-C(10)	123.5(2)	C(21)-C(22)-H(22)	120.1	C(61)-P(2)-C(51)	105.21(11)
N(2)-C(11)-C(12)	116.54(19)	C(24)-C(23)-C(22)	120.8(3)	C(71)-P(2)-C(51)	104.30(10)
C(10)-C(11)-C(12)	120.0(2)	C(24)-C(23)-H(23)	119.6	C(61)-P(2)-Ag(1)	114.09(8)
N(5)-C(12)-N(3)	125.1(2)	C(22)-C(23)-H(23)	119.6	C(71)-P(2)-Ag(1)	118.75(8)
C(51)-P(2)-Ag(1)	110.64(7)	C(54)-C(55)-H(55)	120	C(65)-C(64)-H(64)	119.9
C(52)-C(51)-C(56)	119.1(2)	C(55)-C(56)-C(51)	120.5(2)	C(64)-C(65)-C(66)	120.0(2)
C(52)-C(51)-P(2)	123.35(18)	C(55)-C(56)-H(56)	119.8	C(64)-C(65)-H(65)	120
C(56)-C(51)-P(2)	117.14(18)	C(51)-C(56)-H(56)	119.8	C(66)-C(65)-H(65)	120
C(53)-C(52)-C(51)	120.3(2)	C(62)-C(61)-C(66)	119.5(2)	C(65)-C(66)-C(61)	120.1(2)
C(53)-C(52)-H(52)	119.9	C(62)-C(61)-P(2)	118.91(18)	C(65)-C(66)-H(66)	120
C(51)-C(52)-H(52)	119.9	C(66)-C(61)-P(2)	121.56(18)	C(61)-C(66)-H(66)	120
C(54)-C(53)-C(52)	120.4(2)	C(61)-C(62)-C(63)	120.5(2)	C(72)-C(71)-C(76)	119.2(2)
C(54)-C(53)-H(53)	119.8	C(61)-C(62)-H(62)	119.8	C(72)-C(71)-P(2)	123.20(19)
C(52)-C(53)-H(53)	119.8	C(63)-C(62)-H(62)	119.8	C(76)-C(71)-P(2)	117.56(18)
C(53)-C(54)-C(55)	119.7(2)	C(64)-C(63)-C(62)	119.8(2)	C(71)-C(72)-C(73)	119.9(2)
C(53)-C(54)-H(54)	120.1	C(64)-C(63)-H(63)	120.1	C(71)-C(72)-H(72)	120
C(55)-C(54)-H(54)	120.1	C(62)-C(63)-H(63)	120.1	C(73)-C(72)-H(72)	120
C(56)-C(55)-C(54)	120.0(2)	C(63)-C(64)-C(65)	120.1(2)	C(74)-C(73)-C(72)	120.7(3)
C(56)-C(55)-H(55)	120	C(63)-C(64)-H(64)	119.9	C(74)-C(73)-H(73)	119.7
C(72)-C(73)-H(73)	119.7	O(1S)-Cl(1S)-O(2S)	110.5(2)	O(1U)-Cl(1U)-O(4U)	116.2(14)
C(75)-C(74)-C(73)	119.5(2)	O(1S)-Cl(1S)-O(3S)	110.2(2)	O(3U)-Cl(1U)-O(4U)	107.2(10)
C(75)-C(74)-H(74)	120.2	O(2S)-Cl(1S)-O(3S)	110.54(17)	C(1TA)-O(1TA)-H(1TA)	105.0(19)
C(73)-C(74)-H(74)	120.2	O(1S)-Cl(1S)-O(4S)	108.73(14)	O(1TA)-C(1TA)-C(2TA)	110.1(4)
C(74)-C(75)-C(76)	120.4(2)	O(2S)-Cl(1S)-O(4S)	107.80(14)	O(1TA)-C(1TA)-H(1T1)	109.6
C(74)-C(75)-H(75)	119.8	O(3S)-Cl(1S)-O(4S)	109.01(16)	C(2TA)-C(1TA)-H(1T1)	109.6
C(76)-C(75)-H(75)	119.8	O(2U)-Cl(1U)-O(1U)	111.0(19)	O(1TA)-C(1TA)-H(1T2)	109.6
C(75)-C(76)-C(71)	120.2(2)	O(2U)-Cl(1U)-O(3U)	101.5(13)	C(2TA)-C(1TA)-H(1T2)	109.6
C(75)-C(76)-H(76)	119.9	O(1U)-Cl(1U)-O(3U)	101.1(16)	H(1T1)-C(1TA)-H(1T2)	108.2
C(71)-C(76)-H(76)	119.9	O(2U)-Cl(1U)-O(4U)	117.3(12)	C(1TA)-C(2TA)-H(2T1)	109.5
C(1TA)-C(2TA)-H(2T2)	109.5	C(2TB)-C(1TB)-H(1T4)	109.7	C(2TC)-C(1TC)-H(1T5)	109.9
H(2T1)-C(2TA)-H(2T2)	109.5	H(1T3)-C(1TB)-H(1T4)	108.2	O(1TC)-C(1TC)-H(1T6)	109.9
C(1TA)-C(2TA)-H(2T3)	109.5	C(1TB)-C(2TB)-H(2T4)	109.5	C(2TC)-C(1TC)-H(1T6)	109.9
H(2T1)-C(2TA)-H(2T3)	109.5	C(1TB)-C(2TB)-H(2T5)	109.5	H(1T5)-C(1TC)-H(1T6)	108.3
H(2T2)-C(2TA)-H(2T3)	109.5	H(2T4)-C(2TB)-H(2T5)	109.5	C(1TC)-C(2TC)-H(2T7)	109.5
C(1TB)-O(1TB)-H(1TB)	100(4)	C(1TB)-C(2TB)-H(2T6)	109.5	C(1TC)-C(2TC)-H(2T8)	109.5
O(1TB)-C(1TB)-C(2TB)	109.7(13)	H(2T4)-C(2TB)-H(2T6)	109.5	H(2T7)-C(2TC)-H(2T8)	109.5
O(1TB)-C(1TB)-H(1T3)	109.7	H(2T5)-C(2TB)-H(2T6)	109.5	C(1TC)-C(2TC)-H(2T9)	109.5
C(2TB)-C(1TB)-H(1T3)	109.7	C(1TC)-O(1TC)-H(1TC)	103(4)	H(2T7)-C(2TC)-H(2T9)	109.5

O(1TB)-C(1TB)-H(1T4)	109.7	O(1TC)-C(1TC)-C(2TC)	109(2)	H(2T8)-C(2TC)-H(2T9)	109.5
O(1TC)-C(1TC)-H(1T5)	109.9				

Table S7. Hydrogen bonds (Å), angles (°) for complex Q6.

D-H...A	d(D-H)	d(H...A)	d(D...A)	<(DHA)
O(1TA)-H(1TA)...N(6A)	0.854(15)	2.08(3)	2.902(17)	160(4)

Table S8. IC_{50} values of the isolated complexes.

No.	Comp.	In vitro Cytotoxicity IC_{50} (µM)*	IC_{50} (µM)* for Noncancerous Cells
		MCF-7	MCF-10A
**	**DOX**	4.17±0.2	2.51 ± 2
1	**Q1**	38.35±2.2	100.8 ± 5
2	**Q2**	51.71±2.9	112.4 ± 9
3	**Q3**	13.45±0.9	268.2 ± 7.5
4	**Q4**	80.95±4.1	167.5 ± 4.5
5	**Q5**	46.60±2.6	175.6 ± 14
6	**Q6**	74.80±3.5	123.1 ± 3
7	**Q7**	22.54±1.6	160.2 ± 10

* **IC_{50} (µM)** : 1 – 10 (very strong). 11 – 20 (strong). 21 – 50 (moderate). 51 – 100 (weak) and above 100 (non-cytotoxic) . ** **DOX** : Doxorubicin

Table S9. Antimicrobial activities of the isolated complexes.

Compound	*E. coli*		*S. aureus*		*C. Albicans*	
	Diameter of inhibition zone (mm)	% Activity index	Diameter of inhibition zone (mm)	% Activity index	Diameter of inhibition zone (mm)	% Activity index

Q1	9	34.6	13	54.2	15	55.5
Q2	5	19.2	7	29.2	10	37.0
Q3	10	38.5	14	58.3	21	77.8
Q4	NA	----	3	12.5	5	18.5
Q5	7	26.9	10	41.7	13	48.1
Q6	4	15.4	5	20.8	7	25.9
Q7	12	46.1	16	66.7	19	70.4
Ciprofloxacin	26	100	24	100	----	----
Colitrimazole	----	----	----	----	27	100

Table S10. Molecular docking simulation results with critical interactions between the complexes and CDK2 protein, including HDOCK scores and binding free energies (in kcal/mol)

Compound	**HDOCK**	**ΔG**
Q1	-100.12	-5.16
Q2	-127.55	-5.01
Q3	-143.78	-5.12
Q4	-137.08	-5.13
Q5	-88.98	-5.11
Q6	-93.37	-5.16
Q7	-91.20	-5.23

Table S11. Molecular docking simulation results with critical interactions between complex **Q4** and CDK2 protein, including amino acids, interaction and distance, site–site binding, cation–π, π–π bonds, ionic interactions, and hydrogen bonds

Amino acid	interaction	Distance	Type
A:GLY11:CA - B:1:N	Carbon Hydrogen Bond	3.53342	Hydrogen Bond
A:LYS89:CE - B:1:N	Carbon Hydrogen Bond	2.67498	Hydrogen Bond
B:1:C - A:VAL163:O	Carbon Hydrogen Bond	2.57141	Hydrogen Bond
A:LYS89:NZ - B:1	π-Cation	4.60715	Electrostatic
A:ASP86:OD1 - B:1	π-Anion	3.51767	Electrostatic
A:THR165:OG1 - B:1	π-Donor Hydrogen Bond	3.17736	Hydrogen Bond
A:VAL163:CB - B:1	π-Sigma	3.98452	Hydrophobic
A:VAL164:C,O;THR165:N - B:1	Amide-Pi Stacked	5.45284	Hydrophobic

B:1 - A:VAL164	π-Alkyl	5.4614	Hydrophobic
B:1 - A:VAL163	π-Alkyl	4.88486	Hydrophobic
B:1 - A:LYS88	π-Alkyl	4.22999	Hydrophobic
B:1 - A:LYS89	π-Alkyl	4.23444	Hydrophobic

Table S12: Molecular docking simulation results with critical interactions between the complexes and CDK6 protein, including HDOCK scores and binding free energies (in kcal/mol)

Compound	HDOCK	ΔG
Q1	-92.71	-5.26
Q2	-127.96	-5.05
Q3	-149.39	-5.15
Q4	-138.74	-5.17
Q5	-127.69	-5.12
Q6	-133.11	-5.11
Q7	-136.99	-5.16

Table S13: Molecular docking simulation results with critical interactions between complex **Q4** and **CDK6** protein, including amino acids, interaction and distance, site–site binding, cation–π, π–π bonds, ionic interactions, and hydrogen bonds

Amino acid	interaction	distance	type
A:ASP104:OD2 - B:UNL1	Pi-Anion	3.24484	Electrostatic
A:ALA23:N - B:UNL1	Pi-Donor Hydrogen Bond	4.06318	Hydrogen Bond
B:UNL1 - A:VAL179	Pi-Alkyl	4.96805	Hydrophobic
B:UNL1 - A:ALA23	Pi-Alkyl	4.9053	Hydrophobic
B:UNL1 - A:VAL179	Pi-Alkyl	5.09252	Hydrophobic

Table S14: Molecular docking simulation results with critical interactions between the complexes and **STAT3** protein, including HDOCK scores and binding free energies (in kcal/mol)

Compound	HDOCK	ΔG
Q1	-103.67	-5.63

Q2	-124.94	-5.40
Q3	-122.19	-5.70
Q4	-125.32	-5.37
Q5	-117.45	-5.52
Q6	-102.35	-5.30
Q7	-138.64	-5.52

Table S15: Molecular docking simulation results with critical interactions between complex **Q7** and **STAT3** protein, including amino acids, interaction and distance, site–site binding, cation–π, π–π bonds, ionic interactions, and hydrogen bonds

Amino acid	**Interaction**	**Distance**	**type**
A:MET726:N - B:UNL1:O	Conventional Hydrogen Bond	3.30999	Hydrogen Bond
B:UNL1:O - A:LEU724:O	Conventional Hydrogen Bond	3.22708	Hydrogen Bond
A:PRO725:CA - B:UNL1:O	Carbon Hydrogen Bond	3.63204	Hydrogen Bond
B:UNL1:C - A:THR714:OG1	Carbon Hydrogen Bond	3.70392	Hydrogen Bond
B:UNL1:C - A:TYR657:OH	Carbon Hydrogen Bond	3.54121	Hydrogen Bond
B:UNL1:C - A:MET726:O	Carbon Hydrogen Bond	3.79248	Hydrogen Bond
A:VAL637 - B:UNL1	Alkyl	5.19396	Hydrophobic
A:CYS712 - B:UNL1	Alkyl	4.68668	Hydrophobic
A:PRO715 - B:UNL1	Alkyl	4.70713	Hydrophobic
A:MET726 - B:UNL1	Alkyl	4.78456	Hydrophobic
B:UNL1 - A:ILE659	Alkyl	4.50151	Hydrophobic
A:TYR657 - B:UNL1	Pi-Alkyl	4.95576	Hydrophobic

Table S16 : Molecular docking simulation results with critical interactions between the complexes and **β-lactamases S. AURES** protein, including HDOCK scores and binding free energies (in kcal/mol)

Compound	**HDOCK**	**ΔG**
Q1	-151.14	-5.10
Q2	-150.23	-5.10
Q3	-247.43	-5.09

Q4	-211.14	-5.21
Q5	-184.99	-5.17
Q6	-199.96	-5.09
Q7	-195.22	-5.14

Table S17: Molecular docking simulation results with critical interactions between complex **Q4** and **β-lactamases S. AURES** protein, including amino acids, interaction and distance, site–site binding, cation–π, π–π bonds, ionic interactions, and hydrogen bonds

Interaction	Distance	Type	Category
B:UNL1:O - A:TYR120:O	2.69312	Conventional Hydrogen Bond	Hydrogen Bond
A:SER207:CB - B:UNL1:N	3.06826	Carbon Hydrogen Bond	Hydrogen Bond
B:UNL1:C - A:GLN228:OE1	3.15641	Carbon Hydrogen Bond	Hydrogen Bond
B:UNL1:C - A:GLN228:O	3.60097	Carbon Hydrogen Bond	Hydrogen Bond
A:ARG235:NH1 - B:UNL1	3.66879	Pi-Cation	Electrostatic
A:TYR96:OH - B:UNL1	2.63088	Pi-Lone Pair	Other
A:TYR96 - B:UNL1	4.44585	Pi-Pi Stacked	Hydrophobic
A:TYR120 - B:UNL1	4.9922	Pi-Pi Stacked	Hydrophobic
A:TYR96 - B:UNL1	5.25882	Pi-Pi T-shaped	Hydrophobic
A:TYR96 - B:UNL1	4.26568	Pi-Pi T-shaped	Hydrophobic

Table S18: Molecular docking simulation results with critical interactions between the complexes and **β-lactamases E. COLI** protein, including HDOCK scores and binding free energies (in kcal/mol)

Compound	HDOCK	ΔG
Q1	-127.83	-5.41
Q2	-139.16	-5.14
Q3	-204.45	-5.26
Q4	-175.17	-5.45
Q5	-159.69	-5.36

Q6	-168.47	-5.22
Q7	-163.39	-5.14

Table S19: Molecular docking simulation results with critical interactions between complex **Q4** and **β-lactamases E. COLI** protein, including amino acids, interaction and distance, site–site binding, cation–π, π–π bonds, ionic interactions, and hydrogen bonds

Interaction	Distance	type	Category
A:ARG275:NH1 - B:UNL1:O	2.92698	Conventional Hydrogen Bond	Hydrogen Bond
A:ARG275:NH2 - B:UNL1:O	2.8824	Conventional Hydrogen Bond	Hydrogen Bond
A:ARG275:NH2 - B:UNL1:O	3.22941	Conventional Hydrogen Bond	Hydrogen Bond
B:UNL1:O - A:GLY238:O	2.85719	Conventional Hydrogen Bond	Hydrogen Bond
B:UNL1:C - A:GLU104:OE2	3.46	Carbon Hydrogen Bond	Hydrogen Bond
B:UNL1:C - A:SER70:OG	3.62174	Carbon Hydrogen Bond	Hydrogen Bond
A:GLU104:OE2 - B:UNL1	3.07598	Pi-Anion	Electrostatic
A:MET272:SD - B:UNL1	5.54952	Pi-Sulfur	Other
A:MET272:SD - B:UNL1	5.68107	Pi-Sulfur	Other
A:TYR105 - B:UNL1	3.80862	Pi-Pi Stacked	Hydrophobic
B:UNL1 - A:ALA237	4.44979	Pi-Alkyl	Hydrophobic

References

1. G. M. Sheldrick, *Acta Cryst.,* 2015, ***A71***, 3-8.
2. G. M. Sheldrick, *Acta Cryst.,* 2015, ***C71***, 3-8.
3. P. Müller, *Crystallography Reviews,* 2009, ***15***, 57-83.
4. J. Jimenez, S. Doerr, G. Martinez-Rosell, A.S. Rose, G. De Fabritiis, DeepSite: protein-binding site predictor using 3D-convolutional neural networks, *Bioinformatics*, 2017, **33**(19), 3036-3042.
5. M.D. Hanwell, D.E. Curtis, D.C. Lonie, T. Vandermeersch, E. Zurek, G.R. Hutchison, Avogadro: an advanced semantic chemical editor, visualization, and analysis platform, *Journal of Cheminformatics*, 2012, **4**, 17.

6. Y. Yan, H. Tao, J. He, S.Y. Huang, The HDOCK server for integrated protein-protein docking, *Nature Protocols*, 2020, **15**, 1829-1852.
7. A. Vangone, J. Schaarschmidt, P. Koukos, C. Geng, N. Citro, M.E. Trellet, L. Xue, A.M.J.J. Bonvin "Large-scale prediction of binding affinity in protein-small ligand complexes: the PRODIGY-LIG web server", Bioinformatics, bty816, https://doi.org/10.1093/bioinformatics/bty816
8. Z. Kurkcuoglu, P.I. Koukos, N. Citro, M.E. Trellet, J.P.G.L.M. Rodrigues, I.S. Moreira, J. Roel-Touris, A.S.J. Melquiond, C. Geng, J. Schaarschmidt, L.C. Xue, A. Vangone A.M.J.J. Bonvin "Performance of HADDOCK and a simple contact-based protein-ligand binding affinity predictor in the D3R Grand Challenge 2". J. Comp. Aid. Mol. Des.32, 2018, 175-185.
9. Dassault Systemes BIOVIA. (2020). Discovery Studio Visualizer, Release 2020. San Diego: Dassault Systemes.
10. A. A. Hassoon, R. G. Harrison, N. Nawar, S. J. Smith and M. M. Mostafa, *J. Mol. Struct*., 2020, **1203**, 127240.